

INFORMATION TO USERS

This manuscript has been reproduced from the microfilm master. UMI films the text directly from the original or copy submitted. Thus, some thesis and dissertation copies are in typewriter face, while others may be from any type of computer printer.

The quality of this reproduction is dependent upon the quality of the copy submitted. Broken or indistinct print, colored or poor quality illustrations and photographs, print bleedthrough, substandard margins, and improper alignment can adversely affect reproduction.

In the unlikely event that the author did not send UMI a complete manuscript and there are missing pages, these will be noted. Also, if unauthorized copyright material had to be removed, a note will indicate the deletion.

Oversize materials (e.g., maps, drawings, charts) are reproduced by sectioning the original, beginning at the upper left-hand corner and continuing from left to right in equal sections with small overlaps.

Photographs included in the original manuscript have been reproduced xerographically in this copy. Higher quality 6" x 9" black and white photographic prints are available for any photographs or illustrations appearing in this copy for an additional charge. Contact UMI directly to order.

**ProQuest Information and Learning
300 North Zeeb Road, Ann Arbor, MI 48106-1346 USA
800-521-0600**

UMI[®]

NOTE TO USERS

This reproduction is the best copy available.

UMI[®]

**Localization of N-methyl-D-aspartate Receptor
Subunit 2 mRNAs within the Central Nervous System
of the Weakly Electric Fish *Apteronotus
leptorhynchus*.**

Richard James Finn

Department of Biology
McGill University, Montreal
August, 1999

A thesis submitted to the Faculty of Graduate Studies and Research in partial
fulfillment of the requirements of the degree of Master of Science.

©Richard James Finn 1999



**National Library
of Canada**

**Acquisitions and
Bibliographic Services**

**395 Wellington Street
Ottawa ON K1A 0N4
Canada**

**Bibliothèque nationale
du Canada**

**Acquisitions et
services bibliographiques**

**395, rue Wellington
Ottawa ON K1A 0N4
Canada**

Your file Votre référence

Our file Notre référence

The author has granted a non-exclusive licence allowing the National Library of Canada to reproduce, loan, distribute or sell copies of this thesis in microform, paper or electronic formats.

The author retains ownership of the copyright in this thesis. Neither the thesis nor substantial extracts from it may be printed or otherwise reproduced without the author's permission.

L'auteur a accordé une licence non exclusive permettant à la Bibliothèque nationale du Canada de reproduire, prêter, distribuer ou vendre des copies de cette thèse sous la forme de microfiche/film, de reproduction sur papier ou sur format électronique.

L'auteur conserve la propriété du droit d'auteur qui protège cette thèse. Ni la thèse ni des extraits substantiels de celle-ci ne doivent être imprimés ou autrement reproduits sans son autorisation.

0-612-64352-2

Canada

Table of Contents

Acknowledgements	1
Abstract	11
Résumé	111
Introduction	1
Principles of Electoreception and Electrosensation	6
Electrosensation in <i>A.leptorhynchus</i>	8
The Electrosensory Lateral Line Lobe.....	9
The Molecular Biology of NMDA Receptor Complexes	17
Structural Aspects.....	17
NMDAR Response Characteristics.....	21
Expression of NR2 Subunits is Developmentally Regulated.....	30
Localization of NMDARs at the Post-Synaptic Density.....	32
Materials and Methods	34
Basic <i>E. coli</i> and DNA Protocols.....	34
Preparation of Competent <i>E. coli</i>	37
Transformation of Competent <i>E. coli</i>	39
Subcloning Protocols.....	40
cDNA Library Screening.....	41
High-Stringency Library Screens.....	46
DNA Sequencing Protocols.....	46
Reverse Transcriptase Polymerase Chain Reaction (RT-PCR).....	48
Degenerate RT-PCR.....	48
<i>In situ</i> Hybridization.....	50
Results	57
Cloning of Partial cDNAs encoding <i>Apteronotus</i> NMDAR Subunits.....	57
<i>In situ</i> Hybridization.....	65
Apt. NMDAR2 mRNA Expression in Forebrain Regions.....	65
Apt. NMDAR2 mRNA Expression in Midbrain Regions.....	67
Apt. NMDAR2 mRNA Expression in the ELL.....	68
Discussion	77
Isolation of Partial Apt. NMDAR2 subunit cDNAs.....	77

Distribution of Apt. NMDAR2 mRNAs	78
Summary	88
References	89

Table of Figures

Figure 1: Electoreception.....	7
Figure 2: Anatomy of Electrosensory Lateral Line Lobe.....	1 1
Figure 3: Functional Circuitry of the ELL.....	1 3
Figure 4: NMDAR2 Subunit Topolgy.	2 0
Figure 5: Graphical Representation of Isolated Apt.NMDAR2 cDNAs.....	5 9
Figure 6: Nucleotide and Protein Comparisons, Apt. NMDAR2B.	6 0
Figure 7: Nucleotide and Protein Comparisons, Apt. NMDAR2C.....	6 1
Figure 8: Nucleotide and Protein Comparisons, Apt. NMDAR2D.	6 2
Figure 9: Nucleotide and Protein Comparisons, Degen 5 vs. Apt. NMDAR2B/C/D.....	6 4
Figure 10: Expression of Apt. NMDAR2A and Apt. NMDAR2B mRNAs in Forebrain.	6 6
Figure 11: Expression of Apt. NMDAR2 Subunit mRNAs in Dorsal ELL.....	7 0
Figure 12: Expression of Apt. NMDAR2 Subunit mRNAs in Ventral ELL.	7 2
Figure 13: Expression of Apt. NMDAR2B mRNA in Pyramidal Cell Layer.....	7 3
Figure 14: Differential Expression of Apt. NMDAR2C mRNA across Segments.	7 5
Figure 15: Apt. NMDAR2D mRNA Expressed in a Gradient throughout the Granule Cell Layer.	7 6

Acknowledgements

The completion of this work would not have been possible without the assistance and support of a great many people. I would like to thank Dr. Rob Dunn for introducing me to the fascinating biology of the Brown Ghost and for providing me with the opportunity to work as a member of his research team. Rob's constant enthusiasm, encouragement and genuine love of science were an indispensable source of personal motivation throughout the course of my studies.

I am equally indebted to past and present members of the Dunn laboratory. I would especially like to thank Dr. Daniele Bottai, Mr. Sang Lee and Mr. Asim Rashid for providing me with initial (and continued) training in molecular biology, and Mr. Erik Harvey-Girard for translation of this study's abstract. I am grateful to all members of the lab for their personal concern and stimulating conversation on issues both scientific and inane.

I would also like to acknowledge the invaluable contributions made by Dr. Leonard Maler of the University of Ottawa. This study would not have been possible without Dr. Maler's anatomical expertise and insightful observations concerning the physiology of the Brown Ghost.

In addition, I would like to thank Dr. Michael Ferns for being there to restore balance and perspective when they occasionally went missing (to my mind at least...).

Finally, I would like to thank my parents, James and Lois for providing constant encouragement during the course of this work and never failing to believe that things would work out for the best.

Abstract

Partial cDNAs for each of the four known N-methyl-D-aspartate (NMDA) receptor 2 (NMDAR2A-D) subunits have been cloned from the brain of *A. leptorhynchus* and are found to display a high degree of sequence homology (83-78% amino acid identity) to their mammalian homologues. *In situ* hybridization experiments reveal that each transcript has a distinct expression pattern in the apteronotid central nervous system (CNS) and is present in a "mosaic" distribution within important cell types of the electrosensory lateral line lobe (ELL). Apt. NMDAR2A transcript is expressed in forebrain regions as well as throughout the pyramidal cell layer (PCL) and granule cell layer (GCL) of the ELL. Apt. NMDAR2B mRNA is enriched in mid- and forebrain structures as well as the PCL and GCL of the ELL. Apt. NMDAR2C transcript is largely restricted to cerebellar regions but is also found in the PCL and GCL of the ELL's medial, centromedial, and centrolateral segments. Apt. NMDAR2D mRNA is expressed in sites of cell proliferation and in a segmental gradient within granule cells of the ELL.

Résumé

ADNc partiel pour chacun des quatre sous-unités 2 connues des récepteurs N-méthyl-D-aspartate (NMDAR2 A-D) ont été clônés du cerveau de *A. leptorhynchus* et possèdent un grand degré d'homologie de séquence (83-78% d'acides aminés identiques) comparés à leur homologues mammaliens. Les expériences d'hybridisation *in situ* révèlent que chaque transcript a un patron d'expression distinct dans le système nerveux du poisson et qu'il est distribué en "mosaïque" dans les importants types de cellules du lobe de la ligne latérale électrosensitive (ELL). Le transcript Apt. NMDAR2A est exprimé dans le télencéphale et dans les couches de cellules pyramidales (CCP) et de cellules granulaires (CGL) du ELL. L'ARNm Apt. NMDAR2B est riche dans les structures mésencéphaliques et télencéphaliques ainsi que dans les CCP et CGL du ELL. Celui de Apt. NMDAR2C est fortement restreint aux régions cérébelleuses, mais est aussi retrouvé dans les CCP et CGL du ELL des segments médian, centromédian et centrolatéral. Le transcript de NMDAR2D est exprimé dans les sites de prolifération cellulaire et forme un gradient segmenté dans les cellules granulaires du ELL.

Table of Abbreviations

AM	Amplitude Modulation
BP	Basilar Pyramidal Cell
CCb	corpus cerebelli
CLS	centrolateral segment (ELL)
CMS	centromedial segment (ELL)
CNS	central nervous system
DC	central division of dorsal forebrain
DD	dorsal forebrain, dorsal subdivision
DDmg	magnocellular division of DD
DFL	deep fibre layer
DLd	dorsolateral telencephalon, dorsal division
DML	dorsal molecular layer
DNL	deep neuropil layer
EGm	eminetia granularis medialis
EGp	eminetia granularis pars posterior
ELL	electrosensory lateral line lobe
EOD	electric organ discharge
GCL	granule cell layer
LS	lateral segment (ELL)
MON	medio-octavolateralis nucleus
MS	medial segment (ELL)
NBP	non-basilar pyramidal cell
NMDAR	N-methyl-D-aspartate receptor
nPD	nucleus preaminetialis dorsalis
NR1	N-methyl-D-aspartate receptor, subunit 1
NR2	N-methyl-D-aspartate receptor, subunit 2
PCL	pyramidal cell layer
PL	plexiform layer
PM	pacemaker nucleus
SfF	stratum fibrosum
TeO	optic tectum
TL	torus longitudinalis
TS	torus semicircularis

Tsd

torus semicircularis dorsalis

VCbl

valvula cerebelli pars lateralis

VML

ventral molecular layer

Introduction

The question of how living things are able to sense, and perceive their environments is one of the most intriguing problems being addressed by modern neuroscience. By what mechanisms are organisms able to transform sensory stimuli into a complete perception of their environment?

All sensory systems employ the same basic strategy: energy sources in the environment (sensory stimuli) must be detected by a sensor array and be translated into neuronal electrical energy. The resulting complex patterns of electrical energy must then be directed through a number of processing centres in the central nervous system (CNS) where relevant information can be extracted from incoming spike trains and used to create a meaningful representation of the outside world (Mountcastle, V., 1967).

How is this accomplished? What are the cytoarchitectural and molecular requirements of a network designed to complete these tasks? If a question as complex as this one is to be addressed successfully, it must be approached from a number of different levels of analysis ranging from the organismal to the molecular. Consequently, the choice of a model system that allows such a broad range of experimental opportunities to be exploited is essential.

The electrosensory systems of weakly electric teleost fishes have proven to be excellent models for the study of sensory information processing. These systems, which the animals use to locate objects in their environments and communicate with conspecifics, provide the opportunity to study sensory neural

networks at many levels. Extensive bodies of work that describe the neuroanatomy, electrophysiology, and molecular biology of electroreception exist in conjunction with robust behavioural assays. Taken together, these avenues of investigation promise to provide an unparalleled degree of insight into the functioning of vertebrate sensory systems.

In the case of the weakly electric fish *Apteronotus leptorhynchus*, electrosensory information arrives in the CNS from the periphery and is projected to a hindbrain structure known as the Electrosensory Lateral Line Lobe (ELL) (Carr, C. E. et al., 1986; Heiligenberg, W. and Dye, J., 1982). The ELL is a complex, yet clearly morphologically defined structure, which encompasses a neural network comprised of at least eleven different identifiable cell types (Shumway, C. A., 1989b). Incoming information from primary electrosensory afferents project to a number of topographically organized areas which act as sensory body maps or "Pisciculli" (Heiligenberg, W., 1990). Each of the maps contains a complete complement of cell types and is organized in a laminar fashion, having clearly identifiable molecular, pyramidal cell and granule cell layers. Because of the large existing body of research that has been conducted into the anatomy and physiology of the ELL, it is an ideal structure in which to discern the contribution of receptor function to primary sensory processing.

Glutamate is the major excitatory neurotransmitter in the vertebrate CNS. Among the known glutamate receptors, NMDA receptor (NMDAR) complexes have been the subjects of intense study because of their involvement in neural plasticity and excitotoxicity. (Bliss, T. V. P. and Collingridge, G. L., 1993; McBain, C. J. and Mayer,

M. L., 1994). The NMDAR possesses many characteristics that distinguish it from a stereotypical ligand gated ion channel. NMDARs exhibit a voltage-dependent sensitivity to blockade by magnesium, flux large amounts of calcium, and display a relatively slow and prolonged time course of response to glutamate (Hollmann, M. and Heinemann, S., 1994; McBain and Mayer, 1994).

NMDARs have been implicated in a number of neuronal information processing systems. They contribute to numerous sensory tasks including amplification of auditory responses in the medial geniculate nucleus, involvement in the phasic response to tactile stimulation in the ventrobasal thalamus, and amplification of both excitatory and inhibitory responses in layers V and VI of visual cortex (Daw, N. W. et al., 1993).

NMDARs are particularly interesting in terms of determination of the molecular substrates of information processing because of the great amount of diversity of structure and response characteristics found in native complexes. Functional NMDARs are tetramers composed of two different classes of subunits; an obligatory subunit designated NR1 and at least one of four different species of NR2 subunit (NR2A, B, C and D) (Laube, B. et al., 1998). The NR1 protein arises from a single gene, but is known to exist in a number of different splice isoforms (Zukin, R. S. and Bennett, M. V., 1995). Each of the four NR2 subunits is the product of a different gene; with NR2D being the only of the NR2 subunits known to undergo alternative splicing (giving NR2D-1 and NR2D-2). The response characteristics of NMDA receptor complexes are known to vary greatly depending upon the combinations of NR1 splice isoforms and

NR2 subunits incorporated into a given NMDAR (Ishii, T. et al., 1993; Kutsuwada, T. et al., 1992; Monyer, H. et al., 1994).

It has been established that NMDA-mediated neurotransmission plays an important role in several of the physiological processes involved in the functioning of the ELL. Previous studies have shown that NMDA currents are implicated in the alteration of electric organ discharge characteristics (Dye, J. C. et al., 1989) and several aspects of the descending control mechanisms involved in the control of primary sensory processing at the level of the ELL (Berman, N. J. et al., 1997). Recently, the full-length cDNA encoding the *Apteronotus* NR1 subunit has been cloned, and its distribution within the electrosensory system has been described using *in situ* hybridization techniques. This work has demonstrated that NR1 mRNA is found in high abundance within several important cell types of the ELL (Bottai, D. et al., 1997). In addition, a differential distribution of NR1 splice isoforms was detected (Bottai, D. et al., 1998). Indeed, there is corroborating evidence from pharmacological, and ligand binding assays that NMDAR mediated transmission is integral to the function of this primary sensory relay area (Bastian, J., 1993; Berman et al., 1997; Maler, L. and Monaghan, D., 1991). These findings are important as they indicate that the inherent diversity of the NMDAR is utilized within the cytoarchitecture of the ELL.

In order to further understand the role of NMDAR diversity within the ELL, it is necessary to discern what contribution to the functional construction of the ELL is made by each of the NR2 subunits. To this end, partial cDNAs encoding each of the four NR2 subunits have been obtained by a combination of molecular cloning approaches; fragments of these cDNAs have been used to construct

riboprobes for *in situ* hybridization experiments, and have yielded new information as to the localization of NR2 proteins within the CNS of *Apteronotus* in general, and specifically within the ELL.

Principles of Electroreception and Electrosensation

Electrosensation is a sensory modality by which organisms are able to detect weak electrical emissions or distortions in a self-generated electric field and use this information to perceive their environment. This kind of sensory strategy is known to be employed by monotremes and some species of teleost fishes (Heiligenberg, 1990; Pettigrew, J. D., 1999; Pettigrew, J. D. et al., 1998).

Electroreceptivity, the ability to detect electrical field distortions is thought to be common to all ancestral fish and amphibians.

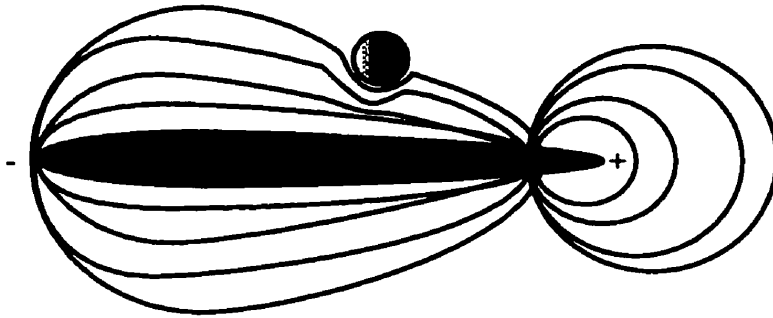
Electrosensation, the ability to actively monitor distortions in a self-generated electric field, is a much less common sensory adaptation. It is now believed that over the course of evolution this ability was lost with the appearance of the holostean fish, only to reemerge in some forms of modern teleosts (Finger, T. E. et al., 1986). Today, electrosensation is known to be employed by at least three forms of modern bony fish: a subset of catfish, the African mormyriforms, and the South and Central American gymnotiforms. *A. leptorhynchus*, is a member of the South American gymnotiform lineage; its common name is the Brown Ghost Knife Fish.

Both mormyrids and gymnotids are similar in the sense that they are true electrosensitive species; they have independently evolved specialized electric organs of neurogenic or myogenic origin from which they emit electric organ discharges (EODs). The emission of an EOD creates an electric field that surrounds the organism. These fish actively monitor distortions in the electric field as a means of gathering sensory information (Figure 1A). The kind of EOD emitted varies among species and may be referred to as

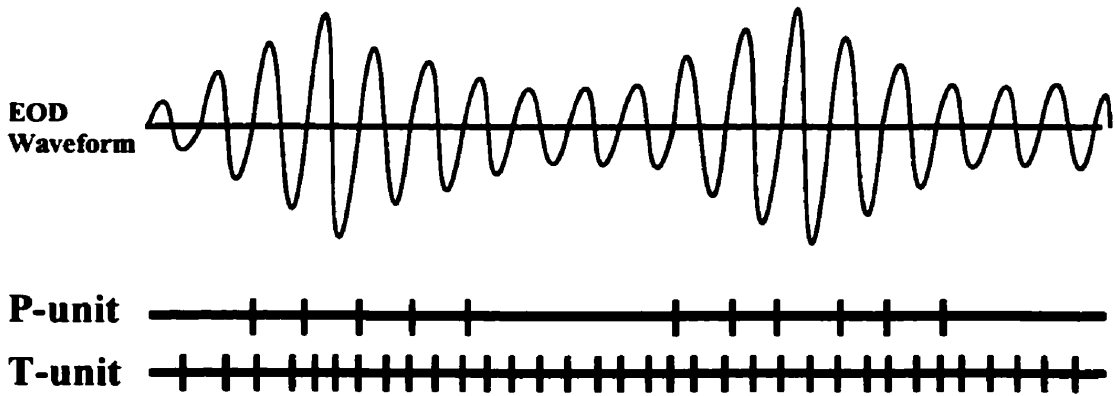
Figure 1: Electroreception

Graphical representation of how amplitude modulations (AMs) and phase distortions affect the firing patterns of amplitude- and phase-coding electroreceptors. **A**, The body of electrosensitive fish is surrounded by an electrical field generated by its EOD. Local conductivity changes caused by the introduction of objects, or interference patterns generated by interaction with conspecific's EODs cause waveform modulations. **B**, Amplitude coding receptors (P-units) spike in response to increases in waveform amplitude. Phase-coding receptors (T-units) respond to zero-crossings.

A



B



being wave-type, or pulse-type depending on the waveform created (Bullock, T. H., 1969). Electrosensitive organisms are able to sense distortions in their surrounding electric fields using an array of specialized cutaneous receptors. Information gained through the interpretation of such distortions of the electric field is used to perform a number of tasks including electrolocation, electrocommunication, and re-calibration of EODs to avoid jamming phenomena while in the presence of conspecifics (Bastian, J., 1981; Kawasaki, M., 1996; Kawasaki, M., 1997).

Electrosensation in *A.leptorhynchus*

A. leptorhynchus is a wave-type gymnotiform species that uses a neurogenic electric organ to emit a quasi-sinusoidal EOD at frequencies of between 600-850Hz. Distortions in the fish's electric field caused by objects or interference with extraneous EODs cause changes in the perceived amplitude and/or phase of the field as detected by the fish. These changes are referred to as amplitude modulations (AMs) or phase-shifts. Disturbances of the fish's electric field are detected by electroreceptors distributed over its body surface. Electroreceptors are specialized structures thought to have evolved from mechanosensory lateral line organs that are capable of detecting changes in transepidermal voltage (Finger et al., 1986; Heiligenberg, 1990). These receptors are classified as being either ampullary or tuberous based on the frequency of stimulation to which they respond preferentially. Ampullary electroreceptors respond maximally to low frequency stimulation ($\approx 40\text{Hz}$) and display an incredible degree of sensitivity,

being able to detect field alterations in the range of several nV/cm. Receptors of this class are found in almost all forms of ancestral fish and are thought to be involved in passive electroreception (Heiligenberg, 1990). Tuberos electroreceptors are almost exclusively found in electrosensitive species, and are maximally responsive to high frequency stimuli which fall within the spectral range of the animal's own EOD. It is the tuberos electroreceptors that are used by electrosensitive species to actively monitor perturbations of their electric fields. Information gathered by this system is propagated to higher brain centres where it is eventually translated into sensory representations.

Tuberos electroreceptors can be further classified as being either probability coders (P-units) or time coders (T-units). P-units fire in an intermittent manner and their firing rates are positively correlated with the amplitude of the stimulus; as a result, they code for information concerning instantaneous amplitude modulation of the EOD. T-units fire in a regular manner once per EOD cycle; their responses are phase-locked to zerocrossings of the EOD waveform and consequently code for phase modulations of the signal (Figure 1B) (Heiligenberg and Dye, 1982).

The Electrosensory Lateral Line Lobe

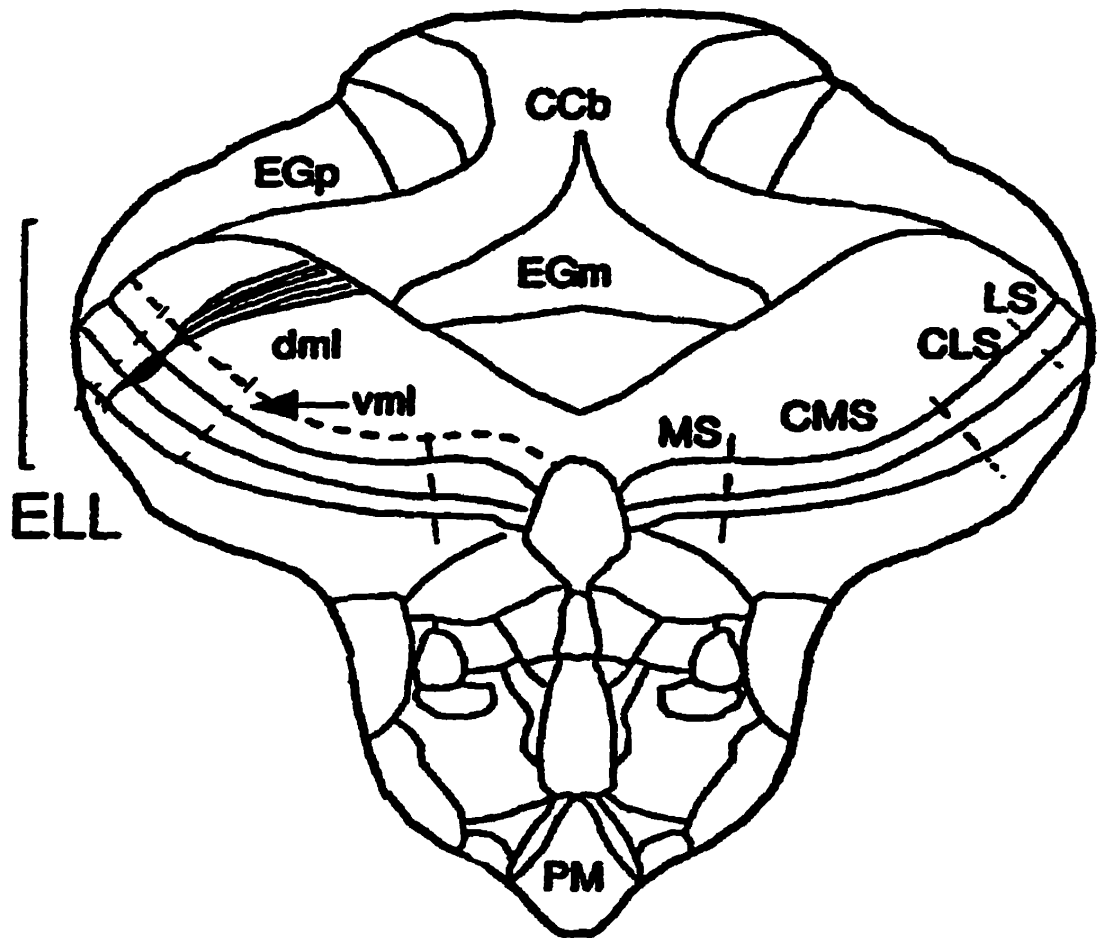
The Electrosensory Lateral Line Lobe (ELL) of the hindbrain is the primary processing centre for electrosensory information in the CNS of *Apteronotus*. The ELL is a specialized brain region thought to have evolved from the lateral line medial octavolateralis nucleus (MON) which is hypertrophied in electrosensitive fish (Montgomery,

J. C. et al., 1995). Extensive characterization of the ELL's cytoarchitecture has revealed it to be a highly laminated structure which is comprised of at least eleven different identifiable cell types (Shumway, 1989b). The laminae of the ELL include a dorsal molecular layer (DML), ventral molecular layer (VML), stratum fibrosum (StF), pyramidal cell layer (PCL), plexiform layer (PIL), granule cell layer (GCL), deep neuropil layer (DNL), and deep fibre layer (DFL). The structure is known to incorporate four discrete regions, which receive topographically organized electroreceptor inputs (Metzner, W. and Juranek, J., 1997; Shumway, 1989b; Shumway, C. A., 1989a). Each of these segments contains a full complement of laminae and cell types and is designated as being medial (MS), centromedial (CMS), centrolateral (CLS), or lateral (LS) according to its location. In *Apteronotus*, there are no known interconnections between each of the four maps (Figure 2) (Carr et al., 1986; Maler, L. et al., 1991).

Ampullary receptor afferents terminate exclusively upon the cells of the MS. Both P-type and T-type tuberous electroreceptor inputs trifurcate at the level of the ELL and project to each of the remaining three maps (CMS, CLS, and LS) (Heiligenberg and Dye, 1982; Shumway, 1989b; Shumway, 1989a). T-units convey phase information via electronic synapses on spherical cells, and this information is then conducted to a higher centre called the torus semicircularis (TS). In the torus, a local neural network conducts phase comparisons. P-units, which conduct information about local AMs project to either basilar or non-basilar pyramidal cells

Figure 2: Anatomy of Electrosensory Lateral Line Lobe.

Relative locations of each of the four topographically organized electroreceptor termination fields, and the laminar organization of the ELL are illustrated. *CCb* corpus cerebelli; *CLS* centrolateral segment; *CLM* centromedial segment; *dml* dorsal molecular layer; *EGp* eminentia granularis pars posterior; *EGm* eminentia granularis pars posterior; *LS* lateral segment; *MS* medial segment; *PM* pacemaker nucleus; *vmf* ventral molecular layer (Adapted from Bastian, 1993). Projections to the somata of non-basilar pyramidal cells (NBPs) are disynaptic via inhibitory granule cells, whereas projections to basilar pyramidal cells (BPs) terminate directly upon basilar dendrites. Efferent projections from BPs and NBPs extend to both the torus and nucleus praeminentialis dorsalis (nPD), where further feature extraction takes place (Figure 3).



Basilar vs. Non-basilar Pyramidal cells

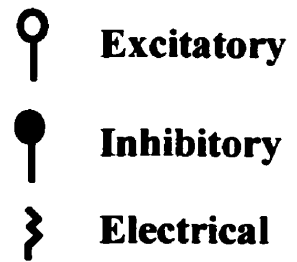
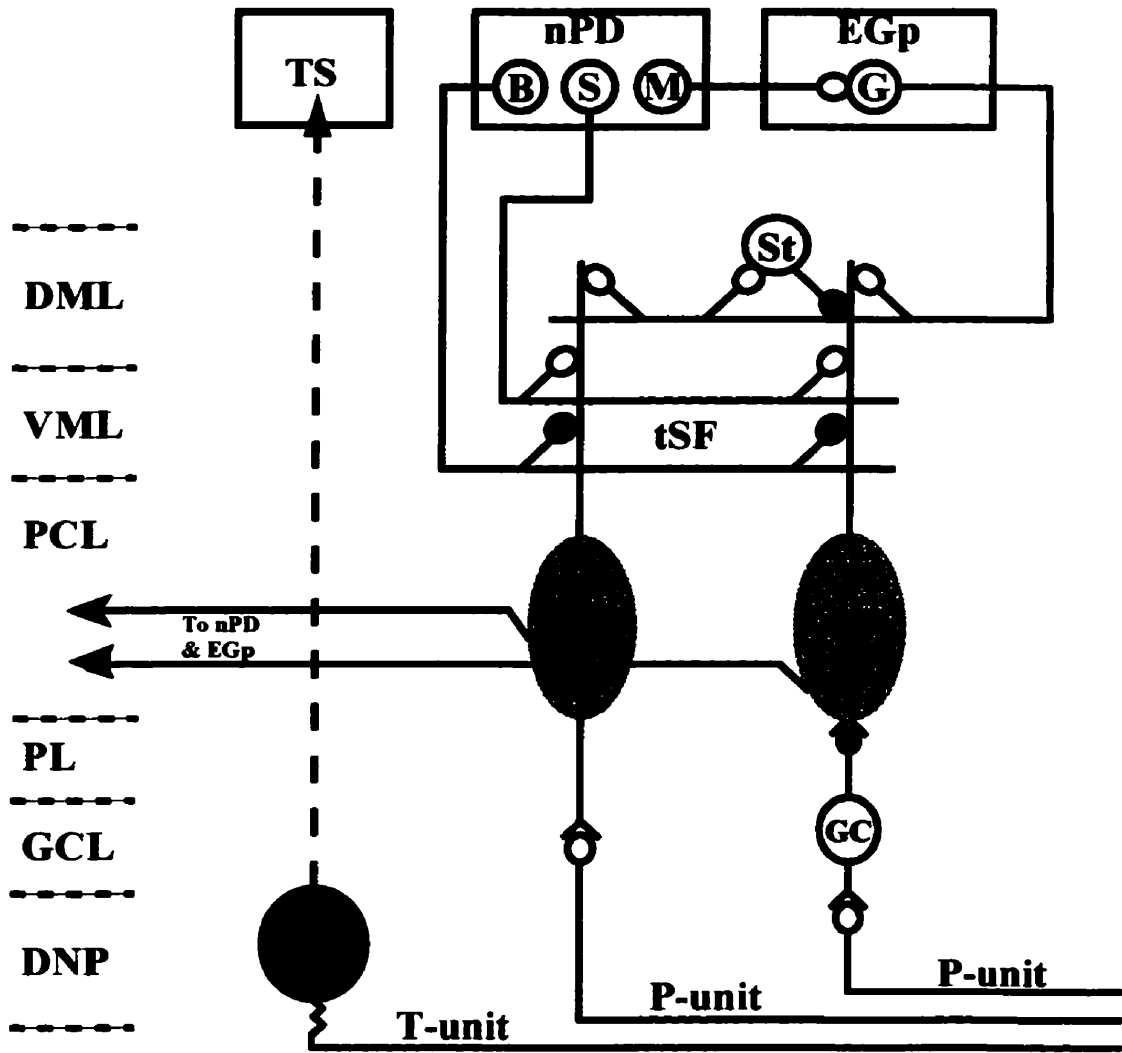
In a manner similar to that of the visual system, the gymnotid electrosensory apparatus utilizes an array of centre-surround receptive fields to facilitate the gathering of spatial and temporal information. In *Apteronotus*, these fields are created by the interplay of BPs and NBPs. As previously described, P-units respond to increases in the frequency of local amplitude modulations with a concomitant increase in their firing rate. Because P-unit input to NBPs is disynaptic via inhibitory contacts (granule cells) NBPs respond to an increase in AM with decreased firing. In the case of the BP, P-unit afferents form excitatory synaptic connections directly upon basilar dendrites. The result is that that BPs respond to increases in AM with an increase in firing rate. In light of these two different responses to excitatory input, BPs are commonly referred to as (E)xcitatory units, and NBPs are known as (I)nhibitory units (Saunders, J. and Bastian, J., 1984).

Response Characteristics Differ across Maps

Physiological studies have revealed that response characteristics of BPs and NBPs to tuberous electrosensory stimulation vary according to the segment in which they are found (Metzner and Juraneck, 1997; Shumway, 1989a). Pyramidal cells of the CMS respond in a tonic manner with a long latency to step increases in AM and show preference to lower frequencies of stimulation. They also have small receptive fields with strong inhibitory surrounds. The result of this combination of properties is

Figure 3: Functional Circuitry of the ELL.

The schematic illustrates efferent and afferent projections to the pyramidal cell layer and the segregation of afferent projections from P-units and T-units. The organization of descending inputs from higher centres involved in gain control and attentional mechanisms is also indicated. *B* bipolar cell; *BP* basilar pyramidal cell; *EGp* eminentia granularis pars posterior; *G* granule cell; *GC* granule cell, type I; *GCL* granule cell layer; *DML* dorsal molecular layer; *DNP* deep neuropil layer; *M* multipolar cell; *NBP* non-basilar pyramidal cell; *nPD* nucleus praeminentialis dorsalis; *PCL* pyramidal cell layer; *PL* plexiform layer; *S* stellate neuron; *SC* spherical cell; *St* stellate cell; *TS* torus semicircularis; *tSF* stratum fibrosum; *VML* ventral molecular layer.



that cells of the CMS appear to be specialized for the extraction of spatial information (at the expense of temporal acuity) from incoming signals. In contrast, LS pyramidal cells respond phasically with a short latency, and show a preference to high frequency stimulation. These cells have been found to have comparatively large receptive fields with weak inhibitory surrounds. This combination of response characteristics makes the pyramidal cells of LS well suited to the extraction of temporal information (at the expense of spatial acuity) (Shumway, 1989b; Shumway, 1989a).

Cells of the CLS display intermediate response characteristics, and seem to show no obvious predisposition towards the optimized extraction of either spatial or temporal information.

Descending input to the ELL

In addition to inputs from primary electroreceptor afferents, pyramidal cells of the ELL receive synaptic inputs from at least two higher brain centres. Projections from the eminentia granularis (EGp) form synapses on the distal apical dendrites of pyramidal cells at the level of the DML. Descending inputs from EGp are implicated in a form of gain control mechanism that allows the organism to adjust the adaptation rates of individual pyramidal cells in response to sustained patterns of stimulation. The result of this kind of modulation is that these cells are able to function over a wide dynamic range of stimulus strengths (Bastian, J., 1986; Heiligenberg, 1990). In addition to projections from the EGp, pyramidal cells receive descending input from the nucleus praeminentialis dorsalis (nPD) to their proximal apical dendrites. These synaptic contacts

are postulated to be important for the operation of an attentional mechanism deemed a "sensory searchlight". Using this searchlight, the organism is able to direct attention towards novel stimuli while "ignoring" reafferent inputs caused by its own behaviours (ventilation, locomotion etc.) (Berman et al., 1997; Crick, F., 1984).

The Role of Glutamatergic Inputs in the ELL

Excitatory amino acid (EAA) neurotransmission has been found to play an important role in the neural circuitry of the ELL (Bastian, 1993). Anatomical studies using radiolabeled ligands have revealed high levels of glutamate binding in the molecular layers of the ELL, suggestive of glutamatergic transmission's importance in the descending control of electroreception (Maler and Monaghan, 1991). Electrophysiological studies have revealed NMDA-mediated components of both descending and primary afferent synaptic contacts (Berman et al., 1997).

The recent cloning of a cDNA encoding the apteronotid NMDAR1 subunit has facilitated *in situ* hybridization studies. This work has revealed that mRNA encoding the NMDAR1 protein is present in a number of important locations in the ELL including granule cells and both basilar and non-basilar pyramidal cells (Bottai et al., 1997). In addition, it has been determined that there is a differential distribution of NMDAR1 splice isoforms among cell types (Bottai et al., 1998). With this established, a number of very important questions are raised about the contribution of NMDAR diversity to the functioning of the ELL. Because of the profound effect of NMDAR2 complement upon the kinetics and response characteristics

of the NMDAR complex, it is vital to discover how they contribute to the functional organization of the ELL. This in turn will help us to begin to understand how this added layer of complexity contributes to the role of NMDARs in sensory processing.

The Molecular Biology of NMDA Receptor Complexes

Fast excitatory neurotransmission in the vertebrate CNS is largely mediated by glutamate. At present, there have been three major classes of ionotropic glutamate receptors identified that are classified according to agonist: N-methyl-D-aspartate (NMDA), α -amino-3-hydroxy-5-methyl-4-isoxazolepropionate (AMPA), and Kainate/kainic acid (KA) receptors. (Hollmann and Heinemann, 1994; McBain and Mayer, 1994).

NMDA receptors (NMDARs) have been implicated in a number of important neural processes including synaptic plasticity and excitotoxicity (Appel, S. H., 1993; Bliss and Collingridge, 1993; Hollmann and Heinemann, 1994; Meldrum, B. and Garthwaite, J., 1990). NMDARs differ from other ligand gated ion channels in several respects: they flux large amounts of calcium, display relatively slow activation kinetics, and require prior membrane depolarization to open (Hollmann and Heinemann, 1994; McBain and Mayer, 1994). It is this last property concerning the need for prior membrane depolarization that enables the NMDAR to function as a molecular coincidence detector (Seeburg, P. H. et al., 1995; Yuste, R. et al., 1999). This ability makes the biology of this receptor particularly interesting from the point of view of understanding the function of neural networks (Nelson, S. B. and Sur, M., 1992).

Structural Aspects

Functional NMDA receptor complexes are heterotetramers that are composed of two obligatory NMDAR1 subunits and two NMDAR2

subunits (Laube et al., 1998; Petralia, R. S. et al., 1994). The mammalian NMDAR1 subunit is a protein of approximately 103 kDa which arises from a single gene and can undergo alternative splicing to give rise to at least nine different isoforms (Hollmann and Heinemann, 1994; McBain and Mayer, 1994; Nakanishi, N. et al., 1992a; Zukin and Bennett, 1995). Eight of these splice variants are the result of the insertion or deletion of one N-terminal and two C-terminal splice cassettes (designated N1, C1 and C2 respectively). Differential splicing of these cassettes can affect various aspects of channel function including susceptibility to pharmacological agents and phosphorylation by intracellular kinases (Nakanishi, S., 1992b). The ninth isoform is truncated and contains only the first 181 NH₂-terminal amino acids; its function in the CNS is unknown (McBain and Mayer, 1994). Interestingly, recent cloning of the apteronotid NR1 has revealed that although N-terminal splicing appears to be conserved in the teleost isoform, C-terminal splicing patterns differ significantly. While the apteronotid NR1 has been shown to undergo splicing of the C1 cassette in a manner similar to that of its mammalian counterparts, no evidence of a C2 cassette splicing has been detected. In addition, the apteronotid NR1 transcript has been found to contain two novel C-terminal splice cassettes designated C1' (19 residues) and C1'' (9 residues) (Bottai et al., 1998).

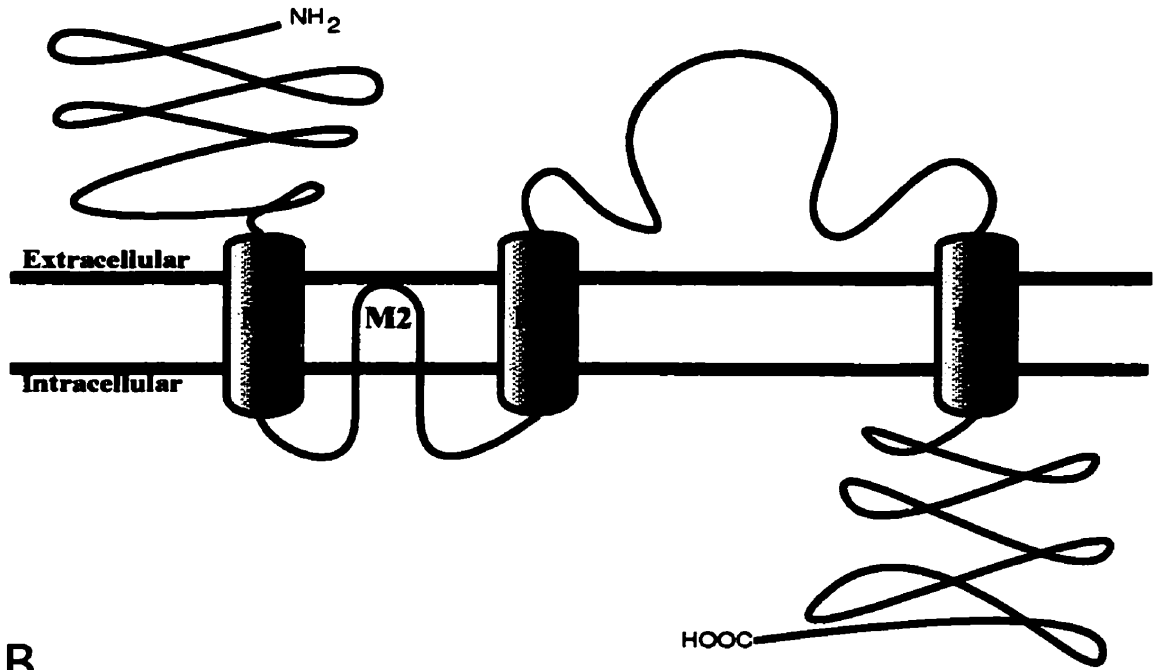
The inherent diversity of NMDAR complexes is augmented by the existence of at least four different NMDAR2 subunits (Ishii et al., 1993; Kutsuwada et al., 1992; Monyer et al., 1994). Each of the NMDAR2 subunits (NR2A, B, C, & D) is the product of a different gene. NMDAR2D is the only species known to undergo alternative splicing

(to give NMDAR2D-1 and NMDAR2D-2). NMDAR2 subunits are large proteins that range in size from 133-163kDa before secondary modification. The topology of completed proteins is such that they contain three transmembrane domains (M1, M3, and M4) and one re-entrant loop (M2) (Figure 4). NMDAR2 subunits are also characterized by large intracellular amino and carboxy-terminal domains.

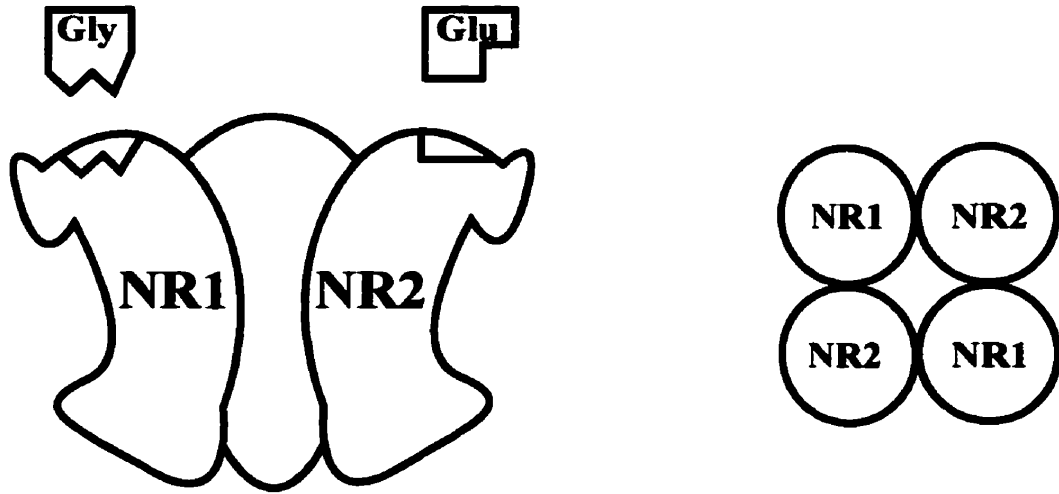
Figure 4: NMDAR2 Subunit Topology.

Schematic representation of NMDAR2 subunit topology. **A**, Membrane topology of a single NMDAR2 subunit is depicted. The subunit's three transmembrane domains (M1, M3 and M4) are illustrated in addition to the protein's re-entrant loop structure (M2), and large amino- and carboxy-terminal domains. **B**, Graphic representation of the proposed tetrameric structure of functional NMDAR complexes, and binding sites for glutamate and glycine.

A



B



NMDAR Response Characteristics

Pharmacology of NMDA Receptors

Glutamate receptors possess a distinctive antagonist pharmacology that has been used to great advantage in their characterization. All NMDARs display a marked sensitivity to the competitive antagonist 2-amino-5-phosphonopentanoic acid (AP5 or APV), and are not inhibited by the AMPA antagonist 6-cyano-7-nitroquinoxaline-2,3-dione (CNQX) (Hollmann and Heinemann, 1994). Native and recombinant NMDARs have been shown to have sensitivity to a number of competitive and non-competitive antagonists which vary in terms of their affinities and modes of action (Hollmann and Heinemann, 1994; McBain and Mayer, 1994). Two of the most popular agents used in studies of NMDAR mediated transmission are the open-channel blocker (+)-5-methyl-10,11-dihydro-5H-dibenzo[a,d]cyclohepten-5,10-imine maleate (MK-801) and D-3-(2-carboxypiperizin-4-yl)-propyl-1-phosphonic acid (D-CPP), a high affinity glutamate antagonist. The pharmacology of NMDARs is complicated by the finding that the incorporation of certain NR2 subunits appears to cause differential sensitivity to antagonists. An example of NR2-specific pharmacology is illustrated in the case of NR2B which has been found to confer sensitivity to the action of ifenprodil (Legendre, P. and Westbrook, G. L., 1991; Williams, K. et al., 1993).

Co-activation of NMDARs by Glutamate and Glycine

NMDAR complexes display a number of unique physiological characteristics that distinguish them from other ligand gated ion channels. One interesting property is that they require the simultaneous binding of both glutamate and glycine to respond maximally. Recent work on the gating kinetics of recombinant NMDARs has indicated that the binding of two molecules of glutamate (to NR2 subunits) and two molecules of glycine (to NR1 subunits) are necessary for optimal response (Benveniste, M. et al., 1990; Benveniste, M. and Mayer, M. L., 1991). The binding sites for these ligands are known to interact allosterically. It is thought that this phenomenon is part of a regulatory mechanism dependant on extracellular glycine concentrations (which are closely regulated in the CNS) (Smith, K. E. et al., 1992).

Modulation by Polyamines, pH, and Reducing Agents

NMDAR complexes are both potentiated and inhibited by the application of polyamines such as spermine and spermidine. The inhibitory action of polyamines is thought to involve binding at the site in the pore of the NMDAR that is involved in the channel's characteristic voltage dependent susceptibility to Mg^{+2} blockade. The inhibitory effect of polyamines upon channel conductance is believed to be the result of charge-screening effects (Rock, D. M. and Mac Donald, R. L., 1992a; Rock, D. M. and MacDonald, R. L., 1992b). The potentiating effects of polyamines are proposed to come about by at least two different mechanisms. In the first instance, it is thought that the binding of polyamines results in the NMDAR increasing its binding affinity for glycine (but not NMDA) (McGurk, J. F. et al.,

1990). A second kind of polyamine mediated potentiation with rapid onset ($\approx 15\text{ms}$) is exhibited by a distinct subpopulation of hippocampal neurons and deemed "glycine-independent" because it is known to occur under saturating concentrations of glycine (Benveniste, M. and Mayer, M. L., 1993). The mode of action of this second form of potentiation is unknown, but may involve the region of the NR1 subunit encoded by the N1 cassette (Durand, G. M. et al., 1992).

Proton concentration is also known to effect the functioning of NMDARs. Increases in proton concentration appear to inhibit the functioning of the NMDAR in a non-competitive manner by decreasing the frequency of channel activation. Proton IC_{50} 's of native NMDA receptors are known to vary according to population (e.g. hippocampal neurons $\text{IC}_{50} = \text{pH}6.6$, cerebellar granule cells $\text{IC}_{50} = \text{pH}7.3$) (Tang, C. M. et al., 1990; Traynelis, S. F. and Cull-Candy, S. G., 1990). Therefore, it is not unreasonable to assume that susceptibility to this kind of inhibition may depend in some measure upon subunit composition.

As with many proteins, NMDARs depend in some measure upon disulfide bonds to create and maintain aspects of their three-dimensional structure. Protein structure is closely tied to both activity and function. Consequently, disruption of these bonds can often result in profound effects. In the case of the NMDA receptor, treatment with the reducing agent dithiothreitol (DTT) which causes disruption of disulfide linkages, leads to a potentiation of the receptor's response to NMDA. This effect can be reversed by subsequent treatment with an oxidizing agent such as 5,5'-dithiobis(2-nitrobenzoic acid) (DTNB) (Aizenman, E. et al., 1989).

Modulation of NMDA Receptors by Protein Kinases

Like many proteins, the NMDA receptor has been found to be subject to phosphorylation by protein kinases (Raymond, L. A. et al., 1993). Early studies of NMDAR mediated neurotransmission in hippocampal neurons revealed that NMDA EPSCs were subject to a phenomenon known as "rundown". Originally, investigators thought that depletion of ATP lead to a decrease in phosphorylation (and therefore activity) of Ca^{+2} transporters in the affected cells. The subsequent rise in intracellular $[\text{Ca}^{+2}]$ was thought to be responsible for the observed inhibition of NMDA currents. It was later demonstrated that the effect was indeed related to the depletion of high-energy phosphates (primarily ATP) within the cell, but that it was observed regardless of the amount of Ca^{+2} present in the cell (MacDonald, J. F. et al., 1989). This was a very important finding because it raised the possibility that NMDA currents may actually be modulated by direct phosphorylation. More evidence to support this idea came from work which demonstrated that NMDA currents could be potentiated by the application of phorbol esters, potent activators of the serine/threonine kinase PKC (Gerber, G. et al., 1989). The role of PKC in the phosphorylation-mediated potentiation of NMDA currents was further established by the observation that activation of PKC via μ -opioid receptors produced the same result as phorbol ester application (Chen, L. and Huang, L. Y. M., 1991).

It is now known that sensitivity to potentiation by PKC is determined by both the splicing pattern of the NR1 subunit, and the species of NR2 subunit incorporated. In the case of the N1 subunit, it was shown that the presence of the N1 splice cassette and absence of both COOH-terminal cassettes (C1 and C2) predispose NMDARs to PKC potentiation (Durand, G. M. et al., 1993; Durand et al., 1992). In addition, it was found that NMDARs that incorporate the NR2A and/or NR2B subunits show a far greater response to PKC activation than those containing NR2C or NR2D do (Kutsuwada et al., 1992). Although the exact mechanism by which PKC phosphorylation works to alter NMDA currents is unknown, it is thought that reduction of sensitivity to Mg^{+2} blockade is involved (Chen, L. and Huang, L. Y. M., 1992).

Studies of long term potentiation (LTP) at hippocampal CA1-CA3 synapses have revealed that NMDARs found in CA1 neurons can also be modulated by the action of various members of the *Src* family of protein tyrosine kinases (PTKs) (O'Dell, T. J. et al., 1991; Wang, Y. T. and Salter, M. W., 1994). This work has indicated that induction of NMDAR phosphorylation via *Src* may be necessary and sufficient for the induction of LTP at these synapses (Lu, Y. M. et al., 1998; Yu, X. M. et al., 1997). In support of this hypothesis, it has been shown that after induction of LTP and subsequent activation of *Src*, the NR2B subunit is the major species of tyrosine phosphorylated protein which can be co-immunoprecipitated from this synapse (Moon, S. I. et al., 1994). It has been proposed that phosphorylation of NR2B by *Src* kinase leads to potentiation of the receptor by relieving its susceptibility to tonic inhibition by zinc ions (Ascher, P., 1998; Zheng, F. et al., 1998).

Recently, it has been demonstrated that yet another protein kinase, calmodulin-dependent protein kinase II (CaMKII) is associated with both the NR1 and NR2B subunits in membrane preparations from rat forebrain (Leonard, A. S. et al., 1999). The actual function of CaMKII in the establishment of LTP via NMDA potentiation is still a matter of some debate, but it is postulated to involve the activation of "silent" AMPA synapses and not directly modulate NMDA currents.

Ca⁺² Dependent Inactivation of NMDARs

Despite the fact that NMDA receptors are known to permit entry of large amounts of Ca⁺² (in the mM range), it is known that influx of Ca⁺² actually has the effect of transiently inhibiting channel function (Legendre, P. et al., 1993). Until recently, the mechanism by which this form of inhibition occurred was unknown. The process is now thought to involve the action of entering Ca⁺² upon the protein calmodulin, and recent studies have shown that calmodulin physically associates with NR1 subunits which contain the C1 cassette *in vivo* (Ehlers, M. D. et al., 1996b). In addition, it has been demonstrated that calmodulin competes for its binding site on NR1 with the cytoskeletal protein α -actinin (Wyszynski, M. et al., 1997). One current model proposes a situation in which the COOH-terminal of C1-containing NR1 subunits are normally associated with the cytoskeleton via α -actinin. In the presence of increased [Ca⁺²], activated calmodulin displaces α -actinin, and facilitates the

transposition of NR1 COOH-terminals into close proximity with the remainder of the NMDAR protein where calmodulin can exert its regulatory effect. The result of this transposition is a 4-fold decrease in the probability of channel opening (Zhang, S. et al., 1998).

Tonic inhibition of NMDA Receptors by Zn^{+2}

NMDA receptors are known to be modulated by a number of divalent cations including Mg^{+2} , Cd^{+2} , and Zn^{+2} (Westbrook, G. L. and Mayer, M. L., 1987). The modulation of NMDARs by Zn^{+2} is of particular interest because this cation is actually released during neural activity and has been shown to accumulate in specific subsets of nerve terminals (Smart, T. G. et al., 1994). At physiological concentrations, Zn^{+2} is known to be implicated in tonic inhibition of NMDA receptors. Zn^{+2} is thought to exert its inhibitory effect through binding to two distinct sites on the NMDAR: a low affinity binding site in the channel pore which causes a voltage dependent inhibition, and a high affinity site elsewhere on the protein which causes a voltage independent inhibition (Christine, C. W. and Choi, D. W., 1990; Legendre, P. and Westbrook, G. L., 1990). Interestingly, binding affinity for Zn^{+2} at the voltage independent site is known to vary with respect to the species of NR2 subunit incorporated. Complexes containing the NR2A subunit display a significantly higher binding affinity for Zn^{+2} at this site than complexes incorporating other NR2s (Chen, N. et al., 1997).

Sensitivity to Mg^{+2} Blockade

One of the most significant properties of the NMDAR complex is its sensitivity to blockade by Mg^{+2} while at resting membrane potentials. It is this “activity dependant” inhibition of channel activity that allows the NMDAR to act as a molecular coincidence detector and makes it of vital importance in the creation of plastic neural networks.

The voltage dependent Mg^{+2} block of NMDARs was originally thought to be the result of Mg^{+2} ions interacting with an asparagine residue within the re-entrant loop segment (M2) of NR2 subunits deemed the *N-site* (Kuner, T. and Schoepfer, R., 1996). The N-site is part of an octopeptide conserved among the various NR2 subunits, and was originally identified in AMPA receptors as an important determinant of permeability to Ca^{+2} and Mg^{+2} (Bunrashev, N. et al., 1992). Studies carried out on the N-site in NR2s have revealed that, as was the case in AMPA receptors, mutation of this asparagine residue to an arginine has a profound effect on the sensitivity of NMDARs to Mg^{+2} blockade. In the case of the NR2 which is most sensitive to block, NR2A, the IC_{50} for Mg^{+2} at $-80mV$ shifts from $7\mu M$ before mutation to $15mM$ afterwards (Kawajiri and Dingledine, 1993; cited in McBain and Mayer, 1994). However, it has become clear that though the N-site is important in the establishment of sensitivity to Mg^{+2} , it is not the only determinant. Construction of chimeric NR2 subunits in which segments of resistant species (e.g.

NR2C) are combined with those of blockade sensitive varieties have revealed that at least three other regions including M1, M3, and the linker between M2 and M3 are involved in Mg^{+2} blockade sensitivity (Edmonds, B. et al., 1995; Kuner and Schoepfer, 1996).

While the exact mechanisms governing sensitivity to Mg^{+2} are still not fully understood, it is clear that the various NR2 subunits clearly show a differential susceptibility. Among the NR2s, NR2A is most sensitive, followed (in order of decreasing susceptibility) by NR2B, NR2D, and NR2C. NMDARs which contain the NR2C subunit display the most marked insensitivity to Mg^{+2} blockade, being able to flux current at potentials as low as $-70mV$ in the presence of $1mM Mg^{+2}$ (Hollmann and Heinemann, 1994). NMDARs containing other NR2 subunits are much more sensitive to this voltage dependent blockade. For example, NR2A containing complexes have an IC_{50} for Mg^{+2} of $\approx 3\mu M$ as compared to NR2C containing complexes which have an IC_{50} of $\approx 15\mu M$ (Seeburg et al., 1995).

NMDAR Kinetics

NMDA receptors differ markedly from other ionotropic glutamate receptors with respect to channel kinetics. AMPA receptors produce EPSCs with rapid onset (time to peak $\approx 200\mu s$) and decay ($\tau = 1-3ms$), this predisposes AMPARs to the faithful transmission of temporal aspects of synaptic stimulation. NMDARs are characterized by much slower kinetic profiles. Parameters such as onset and decay times are known to vary among functional

NMDARs according to which NR1 splice-types and NR2 subunits are incorporated, but in general, they are much slower. NMDARs typically display EPSCs with times to peak on the order of 10ms and decay time constants which range from 120ms (NR1/NR2A) to as long as 4.8s (NR1/NR2D) at a holding potential of -60mV in the presence of 0 Mg^{+2} (Dzubay, J. A. and Jahr, C. E., 1996; Monyer et al., 1994). The result of NMDARs possessing such slow channel kinetics is that they have the ability to integrate patterns of synaptic activity, even at low frequencies of stimulation. These properties give NMDARs the potential to function as good relays of spatial information in sensory systems (Nelson and Sur, 1992).

Expression of NR2 Subunits is Developmentally Regulated

Response characteristics vary greatly depending on the combination of NR1 and NR2 subunits expressed (Buller, A. L. et al., 1994; Vicini, S. et al., 1998). Such attributes as current decay time, maximum current amplitude, sensitivity to pharmacological agents, and susceptibility to Mg^{+2} block all vary according to which combination of NR1 and NR2 subunits are incorporated into a functional channel. Given this large amount of diversity in receptor structure and function, it is not surprising that NMDARs have been shown to have complex patterns of developmentally regulated expression in the CNS (Monyer et al., 1994; Wanatabe, M. et al., 1992). As expected, the expression of NR1 subunit mRNA begins early in embryonic development, and is maintained at high levels in almost all cells throughout subsequent stages. In the case of the

various NR2 subunit mRNAs, patterns of expression differ markedly in terms of location, level, and time course.

NR1, NR2B and NR2D mRNAs are detectable at low levels in the rat CNS as early as embryonic day 14 (E14). By E17, NR1 message is clearly present in a number of structures including cortex, hippocampus and spinal cord. NR2B mRNA is expressed at high levels in cortex, thalamus and spinal cord, and can be seen in the hippocampus and hypothalamus. At this point in time, while NR2D message is expressed at high levels in a number of midbrain structures; it is noticeably absent from the telencephalon.

Expression patterns and levels for NR1, NR2B and NR2D mRNAs remain constant throughout the perinatal period. It is at this time that mRNAs for NR2A and NR2C are first detectable in the CNS, with NR2A message being seen in the hippocampus and NR2C mRNA becoming apparent in the developing cerebellum. As development continues, the expression patterns of NR2 mRNAs become more restricted in terms of location. In the adult animal, mRNA for the NR2A subunit can be detected in the greatest number of brain structures, but its levels are highest in cortex and hippocampus. Message for NR2B becomes largely restricted to forebrain regions, but like NR2A, a high level of expression is maintained within the hippocampus. In the mature CNS, NR2C mRNA becomes almost entirely restricted to cerebellar regions. However, some level of expression is maintained in the both the cells of the corpus callosum, and glia of cortex (layer I). NR2D mRNAs reach peak expression levels in the hypothalamic regions of the CNS about one week after birth and gradually decrease from then on, dropping to

very low levels in the adult (Monyer et al., 1994; Wanatabe et al., 1992).

Specific cell types within the CNS have been found to display changes in NR2 subunit expression both over the course of development and in response to specific patterns of stimulation (Quinlan, E. M. et al., 1999; Sheng, M. et al., 1994; Williams et al., 1993). It has been shown that migrating cerebellar granule cells undergo a developmental switch from expression of NR2A/B containing NMDARs to those containing almost exclusively NR2C (Audinet, E. et al., 1994; Farrant, M. et al., 1994). By the same token, cortical cells have been found to alter their expression of NR2 subunits in response to developmentally relevant stimulation patterns (Carimignoto, G. and Vicini, S., 1992; Flint, A. C. et al., 1997; Kirkwood, A. et al., 1996; Roberts, E. B. et al., 1998).

Localization of NMDARs at the Post-Synaptic Density

A defining characteristic of excitatory synapses in the CNS is the presence of a specialization of the post-synaptic membrane referred to as the post-synaptic density (PSD) (Kennedy, M. B., 1993). The PSD is an electron-dense region of the post-synaptic terminal at which neurotransmitter receptors are selectively clustered in a manner similar to that of acetylcholine receptors at the neuromuscular junction. The clustering of receptors at the PSD is thought to occur by association with elements of the cytoskeleton via accessory proteins (Lin, J. W. et al., 1998; Niethammer, M. et al., 1996). Recently, a great deal of work has been dedicated to the

understanding of how NMDARs become targeted to, and localized at the post-synaptic density.

Through the use of yeast two-hybrid technology and co-immunoprecipitation (co-IP) it has been shown that a number of neurotransmitter receptors and ion channels form associations with various "clustering proteins" (Kim, E. et al., 1995; Roche, K. W. et al., 1999). In the case of the NMDA receptor, interactions with members of the membrane-associated guanylate kinase (MAGUK) family of proteins have been reported. MAGUKs of the PSD-95 family have been shown to interact *in vivo* and *in vitro* with the COOH-terminals of NR1, NR2A, and NR2B subunits (Ehlers, M. D. et al., 1996a; Kim, E. et al., 1996; Kornau, H. et al., 1995).

Recently, it has been demonstrated that interaction of NR2A with PSD-95 can facilitate its phosphorylation by the *Src* family protein kinase *Fyn* (Miyakawa, T. et al., 1997; Sala, C. and Sheng, M., 1999; Tezuka, T. et al., 1999). This finding is of special consequence because it indicates that interaction with MAGUKs may serve not only to localize NMDARs, but also to facilitate their interaction with cellular signaling cascades (Sprengel, R. et al., 1998).

Materials and Methods

Basic *E. coli* and DNA Protocols

Large and Small Scale DNA Preparations

Small scale plasmid DNA preparations were performed using a modified version of the Alkaline Lysis method (Sambrook, J. et al., 1989). Briefly, cultures of *E. coli* were grown overnight at 37°C with shaking (250rpm) in 3ml of standard Luria-Bertani (LB) liquid media (10g tryptone, 5g yeast extract, 10g NaCl per 1L) supplemented with Ampicillin (Sigma) at final concentration of 50µg/ml. Half of the overnight culture was then transferred to a 1.5ml eppendorf tube and spun in a tabletop microcentrifuge at 14,000xg for 30sec at room temperature (RT). The supernatant was then removed by aspiration, and the cell pellet resuspended in 100µl of GTE (50mM Glucose, 25mM Tris-Cl pH 8.0, and 10mM EDTA pH 8.0) supplemented with lysozyme at 10mg/ml. This suspension was incubated at RT for 10min. Cells were lysed by the addition of 200µl of 0.2M NaOH/1% SDS, mixed gently by inversion, and incubated on ice for 5min. Genomic DNA and SDS were precipitated by the addition of 150µl of cold 3M K⁺CH₃COO⁻ (pH 4.8) and incubated on ice for a further 10min. Tubes were then spun at 14,000xg for 10min at RT, and the supernatant transferred to a clean tube. Plasmid DNA was then precipitated by the addition of two volumes of cold 95% EtOH and incubation at -80°C for 15min or -20°C for 1hr. Precipitated plasmid DNA was then spun at 14,000xg for 30min at

4°C, and the supernatant carefully decanted. DNA pellets were allowed to dry for 5min at RT, and were then resuspended in 20-50µl of TE 10:1 (10mM Tris-Cl pH 8.0, 1mM EDTA pH 8.0).

Large-scale plasmid preparations were performed using a modified Alkaline Lysis method supplemented with further purification by CsCl gradient centrifugation. 10ml overnight cultures of *E. coli* were grown at 37°C with shaking (250 rpm) in LB media supplemented with Ampicillin (50µl/ml). These cultures were then used to inoculate 1L of LB supplemented with Ampicillin (50µg/ml). Large cultures were then grown overnight at 37°C with shaking (250rpm). The following day, cultures were transferred to 4x250ml GSA centrifuge tubes and spun at 4,000xg for 10min at 4°C in a Beckman model J2-21M centrifuge. After removal of the supernatant, cell pellets were resuspended in 36ml of GTE (total volume). Once the cell pellet was resuspended completely, 2ml of lysozyme (10mg/ml) were added and the mixture was incubated at RT for 10 min. Cells were lysed by the addition of 80ml of room temperature 0.2M NaOH/1% SDS (prepared fresh), mixed by inversion, and incubated on ice for 5min. Genomic DNA and SDS were precipitated by the addition of 40ml of cold 5M K⁺CH₃COO⁻ (pH 4.8) and incubated on ice for 15min. The mixture was then spun at 6,000xg for 15min at 4°C, and the supernatant strained through gauze into a 250ml-graduated cylinder. The volume of the supernatant was determined and 0.6 volumes of isopropanol added. Plasmid DNA was precipitated by incubation at -20°C for at least 1.5hrs. Samples

were then spun at 6,000xg at 4°C for 20min. The supernatant was then carefully decanted, and the remaining DNA/RNA pellet allowed to dry; excess supernatant was carefully removed by swabbing with a clean Kimwipe. The resulting pellet was then resuspended in 10ml of TE 10:10 (10mM Tris-Cl pH 8.0, 10mM EDTA pH 8.0). This solution was titrated with 1M Tris-Cl pH 8.0 until a final pH of 7.0-8.0 was attained. The solution was then transferred to a SS34 centrifuge tube, and its volume noted on transfer. Next, CsCl was added to a final concentration of 1.1g/ml, and mixed well. Once mixed, 200 μ l of ethidium bromide (EtBr) (10mg/ml) was added to the solution, and it was incubated on ice, in the dark for 30min. After this incubation, the samples were spun at 10,000xg for 30min at 4°C and the supernatant carefully transferred to Beckman quickseal tubes and balanced to within 100mg. The samples were then spun in a Beckman L8-80M ultracentrifuge at 55,000rpm (Ti70.1 rotor) for 24hrs at 14°C.

Following ultracentrifugation, plasmid bands were carefully removed and transferred to clean tubes. CsCl and EtBr were then extracted from the sample using water-saturated butanol. Extracted samples were then purified on a BioGel™A-50M column. Fractions were assayed for DNA content and purity using a Shimadzu UV160U spectrophotometer. Finally, DNA was aliquoted in appropriate amounts and precipitated using Na⁺CH₃COO⁻ at a final concentration of 0.3M and 3 volumes of molecular biology grade 95% EtOH; samples were then stored at -20°C.

Preparation of Plasmid DNA for Automated Sequencing

Plasmid DNA samples used for automated sequencing were prepared using the Promega Wizard™ or Wizard SV™ DNA miniprep system. Overnight cultures were grown in 3ml of LB liquid media supplemented with Ampicillin (50µg/ml). Plasmid preparations were then carried out according to the manufacturer's instructions. Final resuspension of DNA pellets was in 30µl H₂O.

Preparation of Competent *E. coli*

Single colonies of the appropriate bacterial strain (XL1-Blue MRF' [Stratagene] or DH5α [Life Technologies]) were used to inoculate 5ml of LB media and grown overnight at 37°C with shaking (250rpm). The following day, 400ml of LB media was inoculated with 4ml of overnight culture and grown at 37°C with shaking (250rpm) until an OD₆₀₀ of approximately 0.375 was obtained. The culture was then aliquoted into eight pre-chilled 50ml Falcon™ tubes and incubated on ice for 10min. Cells were then centrifuged at 1,600xg for 7min at 4°C, and the supernatant was carefully removed. Cell pellets were then gently resuspended in 10ml of ice-cold CaCl₂ solution (15% Glycerol w/w, 10mM PIPES pH 7.0, sterilized by autoclaving). Resuspended cells were then spun at 1,100xg for 5min at 4°C, and the supernatant was carefully removed. Pellets were then gently resuspended in 2ml of ice-cold CaCl₂ solution and incubated on ice for 16-18hrs. Cell suspensions were then aliquoted in appropriate volumes into sterile microcentrifuge tubes and stored

at -80°C until needed. Transformation efficiency was assessed by transformation with serial dilutions of a known concentration of Plasmid DNA.

Transformation of Competent *E. coli*

Competent *E. coli* (100 μ l) were aliquoted into pre-chilled, sterile 5ml glass culture tubes or 15ml Falcon™ tubes and gently mixed with the appropriate amount of plasmid DNA (\approx 5ng) or ligation reaction (half of reaction volume); these mixtures were then incubated on ice for 1hr. Samples were then heat-shocked at 42°C for 45sec and incubated on ice for a further 2min. 200 μ l of LB media was then added to each tube, and cultures were allowed to grow at 37°C with shaking (250rpm) for 45min. Cell suspensions were then spread onto LB-Agar plates supplemented with Ampicillin (50 μ g/ml) and allowed to dry covered at RT for 30min. Plates were then inverted and incubated at 37°C for 18-24hrs.

Note: If transformants were to be assayed for presence of insert by Blue/White selection, LB-Agar plates were spread with a mixture of isopropylthiogalactoside (IPTG) and X-Gal (chromogenic lactose analog) (10 μ l IPTG [200mg/ml], 50 μ l X-Gal [50mg/ml], 40 μ l LB) and allowed to dry at 37°C for 30min prior to cell plating.

Subcloning Protocols

Subcloning of DNA Fragments

DNA fragments were prepared for subcloning by digestion with the appropriate restriction enzymes and purification on 0.7%-1.2% agarose gels. Appropriate fragments were visualized using EtBr staining and viewed under low intensity UV. UV exposure was kept to the minimum necessary for band excision. After excision, DNA fragments were purified using the QIAquick™ DNA gel purification kit according to the manufacturer's instructions. Final resuspension of fragments was in an appropriate volume of dH₂O.

Digested vector and insert DNA were combined in 10μl ligation reaction mixtures containing 3 units of T4 DNA Ligase (3u/μl, Promega), 1x T4 Ligation Buffer (30mM Tris-Cl, 10mM MgCl₂, 10mM dithiothreitol [DTT], and 1mM ATP), and the appropriate volume of dH₂O. Reactions were then incubated at 16°C for 18-24hrs.

Note: Unless indicated, all routine subclonings were into the pGEM-7z(+) vector (Promega).

Subcloning of Polymerase Chain Reaction (PCR) Products

After gel purification, PCR products were subcloned using the pGEM-T vector system (Promega) in accordance with the manufacture's instructions.

cDNA Library Screening

***Apteronotus* brain cDNA Libraries**

Two *Apteronotus* brain cDNA libraries were constructed by Dr. Daniele Bottai from poly A-enriched whole brain RNA using a Hybri-Zap™ library construction kit (Stratagene). One of the libraries was size-selected for inserts 1-2kb in size (Dano 1/2), and the other for inserts of 2-10kb in size (Dano 2/10) (Bottai et al., 1997, 1998).

Preparation of dsDNA Probes

Initial screening of the Dano 1/2 and Dano 2/10 libraries was carried out at low stringency using a DNA fragment corresponding to the full-length sequence of the *R. norvegicus* NMDAR2C subunit (gift of Dr. P. H. Seeburg). The DNA fragment was excised from the pBluescript vector (Stratagene) by double digestion with the restriction enzymes BamHI and EcoRI, and then electrophoresed on a 0.8% agarose gel. The appropriate fragment (≈ 4.5 kb) was cut out, and purified using Amicon™ spin-columns. After column purification, the DNA samples were extracted once with phenol:chloroform:isoamyl alcohol 25:24:1, and then twice with diethyl ether. After ether extraction, samples were reprecipitated with $\text{Na}^+\text{CH}_3\text{COO}^-/\text{EtOH}$ at -20°C for ≥ 1 hr. The DNA was then spun down at 14,000xg for 30min at RT and resuspended in an appropriate volume of dH₂O.

Low Stringency Screening of Dano 1/2 and Dano 2/10 Libraries

Plating and Titreing of cDNA Libraries

λ phage containing the cDNA libraries were prepared for screening by infection of LE392 or XL1-Blue MRF' *E. coli*. Briefly, bacterial cultures were grown at 37°C with shaking (250rpm) to early log-phase ($OD_{600} \approx 0.4$) in the presence of maltose and $MgSO_4$ (5ml LB, 50 μ l 20% w/w maltose [filter sterilized], 50 μ l 2M $MgSO_4$, 100 μ l overnight culture). Serial dilutions of phage were then gently mixed with 600 μ l of log-phase cells in a 15ml sterile culture tube and allowed to incubate without agitation at 37°C for 30min. After infection, 6-8ml of molten ($\approx 50^\circ C$) λ top agarose (10g tryptone, 8g NaCl, 6g agarose per 1L) was added to cells and briefly mixed. The mixture was then spread on 150mm bacteriological plates (Fisher) containing λ plate agar (10g tryptone, 2.5g NaCl, 10g agar) warmed to 37°C. After the top agarose was allowed to harden, plates were inverted and incubated at 37°C for 16-18hrs.

The following day, infection efficiency was determined, and the procedure was repeated to obtain a plating density of $\approx 50,000$ pfu/150mm plate.

Nitrocellulose Filter Lifts and Hybridization

After plating at the appropriate density λ phage plaques were transferred to nitrocellulose membranes (Millipore HAHY filters,

0.22 μ m) with replicant lifts being made for initial (150mm plate) screens. Plates were allowed to cool to RT, and then overlaid with nitrocellulose filters for the appropriate times (45sec first lift, 1.5min replicant lift). Filters were then allowed to dry at RT for \approx 45min. After drying, filters were treated for 45sec in denaturation solution (1.5M NaCl, 0.5M NaOH), 5min in neutralization solution (0.5M Tris-Cl, 1.5M NaCl), and 5min in 2x Standard Saline Citrate (SSC) (0.3M NaCl, 30mM Na citrate). The filters were then allowed to dry at RT, and subsequently baked in an isotemp oven at 80°C for 2hrs.

After baking, filters were further prepared by pre-hybridization for 1hr at 37°C with gentle shaking. The prehybridization solution (100ml) consisted of: 35ml deionized formamide, 15ml dH₂O, 500mg skim milk powder, 100mg total yeast RNA (Sigma), and 250 μ l sonicated salmon sperm DNA (10mg/ml, boiled for 5min) mixed with 50ml 2x hybridization solution (5% SDS w/w, 266mM glycine, 1.8M NaCl, 25mM Tris-Cl pH 8.0, 2.5mM EDTA pH 8.0). The result is a 1x hybridization solution containing 35% formamide v/v.

Once filters were pre-hybridized for \geq 1hr, the solution was removed and replaced with fresh 1x hybridization solution containing the [α -P³²] radiolabeled DNA probe at a concentration of \approx 1x10⁶cpm/ml. Labeling of the dsDNA probe was accomplished using the Prime-It RT™ random primer labeling kit (Stratagene) according to the manufacturer's instructions. Labeled probe was denatured by the addition of NaOH to [0.2]Final and incubation at

37°C for 15min. Hybridization was allowed to proceed at 37°C overnight with gentle agitation.

Washing Sequences

After hybridization, filters were washed in the following sequence: 2xSSC/1% SDS for 15min at RT, and twice in 2x SSC/1% SDS for 30min at 55°C. After the final wash filters were allowed to dry at RT, covered with a single layer of plastic wrap, and apposed to Biomax XAR film (Kodak) overnight at -80°C.

Purification of Hybridization-Positive Phage Clones

After development of films, positive phage clones were identified by comparison of hybridization patterns found on original and replicant nitrocellulose. Agar plugs containing positive clones were removed from the original 150mm plates and transferred to sterile microcentrifuge tubes containing phage suspension medium. After incubation at RT for 3-4 hrs, positive phage were re-plated on 15mm bacteriological plates (Fisher) and screened again. This process was repeated until isolated positive phage plugs could be obtained.

Phage Insert Excision Protocol

Once single, isolated hybridization-positive plaques had been obtained, clones were excised using Ex-Assist™ interference resistant f1 helper phage (Stratagene). Overnight 10ml LB cultures

of XL1-Blue MRF' and XLOLR *E. coli* (Stratagene) were grown at 30°C. The following day, both cultures were spun down at 500xg for 10min at 4°C and resuspended in cold 10mM MgSO₄ to a final OD₆₀₀ of ≈1.0. 3x10ml LB cultures of each strain were begun and grown at 37°C with shaking (250rpm) until they reached an OD₆₀₀ of ≈0.3-0.4. Cells were then spun at 500xg for 10min at 4°C and once more resuspended in cold 10mM MgSO₄ (XL1-Blue MRF' to OD₆₀₀ ≈5.0, XLOLR to OD₆₀₀ ≈1.0).

Co-infection of XL1-Blue MRF' cells was achieved by mixing 40μl of cells with one-half of the purified phage suspension (≈20-25μl) and 2μl of Ex-Assist™ f1 helper phage; this mixture was incubated without agitation at 37°C for 30min. Following co-infection, 5ml of LB media was added to each tube and cells were allowed to grow at 37°C with gentle agitation (100rpm) for 3-8hrs. Cell suspensions were then transferred to sterile microcentrifuge tubes and incubated at 70°C for 20min to facilitate the release of excised phage. Samples were spun at 500xg for 20min at RT to pellet cellular debris, and supernatants were transferred to clean microcentrifuge tubes. 20μl of excised phage suspension was then mixed with 200μl of XLOLR cells and incubated at 37°C for 20min. The mixture was then spread on LB-agar plates supplemented with Ampicillin (50μg/ml). Plates were inverted and incubated at 37°C overnight.

The following day, excised clones were assayed for insert presence and size by restriction digest with EcoRI.

High-Stringency Library Screens

In cases where cDNA libraries were screened at high stringency to facilitate the extension of previously obtained clones, the procedures followed were identical to those outlined above with the following exceptions: Hybridizations were carried out at 42°C, 1x hybridization solution was 50% deionized formamide by volume, and high-temperature washes were carried out at 60-65°C.

DNA Sequencing Protocols

Subcloning

Once isolated, cDNA clones were excised from library phagemid vectors by digestion with EcoRI (or other appropriate endonuclease[s]) and subcloned into the pGEM-7z(+) vector (Promega) for primary nucleotide sequence determination.

When warranted by insert size, nested deletions of cDNA clones were created using the Erase-A-Base™ Exonuclease III/S1 nuclease kit (Promega).

Manual Sequencing

Plasmid DNA was prepared using the standard alkaline lysis miniprep protocol (supplemented with a LiCl RNA precipitation step), and resuspended to a final concentration of $\approx 1\mu\text{g}/\mu\text{l}$ in dH₂O. Manual sequencing was then performed on the dsDNA template using the Sequenase 2.0™ dideoxy terminator core kit (United States

Biochemical) with [α -S³⁵] dATP as the radiolabel to be incorporated. Initial sequence data was then obtained from all clones using T7 and SP6 sequencing primers. Reactions were run on 5% acrylamide/8M urea gels and apposed to Biomax XAR film overnight at RT.

Automated Sequencing

Plasmid DNA was prepared using Wizard™ or Wizard SV™ miniprep kits (Promega) and resuspended at a final concentration of $\approx 1\mu\text{g}/\mu\text{l}$ in dH₂O. Sequencing reactions were then carried out on dsDNA templates using the 7-deaza Thermosequense Core Cycle Sequencing Kit (United States Biochemical/Amersham Biotech) according to the manufacturer's instructions. Initial sequence data was obtained from all clones using M13 forward, and M13 reverse sequencing primers. Reactions were analyzed using the OpenGene™ automated sequencing system version 2.0 (Visible Genetics).

Sequence Analysis

All analysis of primary sequence was carried out using the DNASTAR molecular biology software package. Applications included: sequence editing, contig assembly and construction of restriction maps. Initial searches for sequence homology were carried out using the National Centre for Bioinformatics (NCBI) on-line Basic Local Alignment Tool (BLAST) (<http://www.ncbi.nlm.nih.gov/blast>).

Reverse Transcriptase Polymerase Chain Reaction (RT-PCR)

RT-PCR was employed in routine amplification of *Apteranotus* NMDAR2 subunit fragments using cDNA constructed from whole brain total RNA. All Reverse Transcription (RT) reactions were carried out using a Perkin-Elmer RNA PCR core kit according to the manufacturer's instructions for reverse transcription using random hexamers. After production of cDNA, PCR amplifications were undertaken using conditions optimized for both primer annealing temperature and MgCl₂ concentrations. In all cases, Amplitaq™ (Perkin-Elmer) was the thermostable polymerase used. All PCR amplifications were performed on a Robocycler Gradient 48™ thermal cycler (Stratagene). Unless otherwise noted, typical cycling conditions were:

94°C, 2min.				1 cycle
94°C, 1min.	45-65°C, 1min.	72°C, 1min.		35 cycles
72°C, 1min				1 cycle

Degenerate RT-PCR

A degenerate RT-PCR approach was used to obtain a 154bp fragment of the Apt. NR2A subunit for subsequent use as a probe in *in situ* hybridization studies. This strategy involved the amplification of a 154bp fragment of the NR2 subunit, which is divergent among the various NR2 genes. Amplification was achieved using degenerate primers corresponding to two regions flanking the 154bp which were highly conserved among the various NR2s at

the amino acid level. The primers used and their corresponding amino acid sequences were: NR2 Degen 1 (5'- TTY GGI ACI GTI CCI AAY GGI -3' ; F G T V P N G), and NR2 Degen 2 (5'- IGC RTC RTA DAT RAA IGC RTC -3' ; A D Y I F A D) where Y= pyrimidine, R= purine, D=T/A/G, and I=inosine. Amplification of this fragment was undertaken in two rounds. The first amplification was carried out using a MgCl₂ concentration of 4mM and both primers at a concentration of 0.6μM.

Cycling conditions were:

95°C, 2min.	1 cycle
95°C, 1min. 49°C, 1min. 72°C, 1min.	35 cycles
72°C, 7min.	1 cycle

This round of amplification yielded produced a complex banding pattern on a 1.2% agarose gel. However, one of the observed products was a band of the correct size (≈154bp). This fragment was excised and purified using the QIAquick™ Gel Purification Kit (Qiagen). The sample was then reprecipitated in 0.3M Na⁺CH₃COO⁻/95% EtOH overnight at -20°C.

The following day, the sample was spun down and resuspended in 10μl of dH₂O. The second round of PCR was carried out using 2μl of the original reaction as template. Amplification was carried out using a MgCl₂ concentration of 4.0mM and both primers at a concentration of 0.6μM.

Cycling conditions were:

95°C, 2min.	1 cycle
95°C, 1min. 49°C, 1min. 72°C, 1min.	35 cycles
72°C, 7min.	1 cycle

This amplification yielded a single product of ≈ 154 bp. The fragment was excised, purified using the QIAquick™ Gel Purification Kit (Qiagen) and reprecipitated at -80°C for 20min. The sample was then resuspended in $10\mu\text{l}$ of dH_2O and subcloned into pGEM-T for primary sequence analysis.

In situ Hybridization

Perfusion

Brains were harvested from male *Apteronotus* that ranged in length from 10-15cm. Fish were deeply anesthetized in a solution of MS-222 (Sigma), and then transferred to a perfusion apparatus where they were respired with a solution of MS-222 and dH_2O to ensure maintenance of anesthesia. The animals were then perfused intracardially with ≈ 25 ml of 1x Phosphate Buffered Saline (PBS) (8g NaCl, 0.2g KCl, 1.44g Na_2HPO_4 , 0.24g KH_2PO_4 per 1L, adjust pH to 7.4 with HCl), followed by ≈ 50 ml of 4% Paraformaldehyde/1x PBS. After perfusion with fixative, brains were carefully removed and post-fixed in 4% Paraformaldehyde/1x PBS for 2hrs at 4°C . Tissue

was then transferred to a solution of 4% Paraformaldehyde/1x PBS/10% Sucrose and incubated overnight at 4°C.

The following day, brains were embedded in Cryomold™ biopsy molds (TissueTek) with OCT mounting media (TissueTek) at -55°C and stored in a sealed box containing desiccant at -80°C until needed.

Sectioning

Tissue was sectioned at between 10-12µm in a cryomicrotome maintained at a temperature of -25°C. Sections were collected on Fisherbrand Superfrost™ slides coated with poly-L-lysine. After sectioning, slides were immediately transferred to a 40°C slide-warmer for 10min. The samples were then post-fixed in 4% Paraformaldehyde/1X PBS for 45min at 4°C. After post-fixation, sections were dehydrated in ascending alcohols (50%, 70%, 95%, 100%, 3min each), placed on a 40°C slide-warmer for 10min, and then stored at -80°C with desiccant.

Preparation of RNA Probes

In situ hybridizations were carried out on coronal sections of *Apteronotus* brain using [α -S³⁵] CTP labeled riboprobes. For each experiment, probes were prepared immediately before use from linearized dsDNA templates. Templates were constructed using PCR amplification, or restriction digest as indicated in the following table.

Gene	Primer Pairs/Enzyme used for Template Preparation	Vector	Size (bp)
NR1	As per (Bottai et al., 1997)	pGEM-T	212bp
NR2A	NR2 Degen 1 NR2 Degen 2	pGEM-T	154bp
NR2B	2B 3' Upper 2B 3' Lower	pGEM-T	203bp
NR2C	2C 3' Upper 2C 3' Lower	pGEM-T	243bp
NR2D	Apo I digest of Clone 16	pGEM-7z(+)	251bp

Primer Sequences (5'->3')

NR2 Degen 1	TTY GGI ACI GTI CCI AAY GGI
NR2 Degen 2	IGC RTC RTA DAT RAA IGC RTC
2B 3' Upper	AAC GGT TCG CCC CAC AGC
2B 3' Lower	CGG CAC GAG GCA GGA ACT
2C 3' Upper	GTG GGC CTT GGG ATG ACC
2C 3' Lower	GGA CAA TGC CAC TAA GAC C

After subcloning and sequence verification, templates were linearized with the appropriate restriction enzyme, run on 0.7% agarose and purified using the QIAquick™ gel purification system. After purification, templates were extracted once with

phenol:chloroform:isoamyl alcohol (25:24:1), twice with diethyl ether and reprecipitated overnight at -20°C.

Prior to hybridization, riboprobes were transcribed under the following conditions:

10x Transcription Buffer	1 μ l
RNase Inhibitor (7.5U/ μ l)	0.5 μ l
ATP/GTP/UTP mix (2.5mM)	2 μ l
CTP (100 μ M)	0.5 μ l
Template (1 μ g/ μ l)	2 μ l
T7/SP6 RNA Polymerase (20U/ μ l)	1 μ l
[α -S ³⁵] CTP	3 μ l

Reactions were gently mixed and incubated at 37°C for 2.5hrs. 7.5U of DNase I (Pharmacia) was then added to each reaction and incubation was allowed to proceed at 37°C for a further 30min. After DNase digestion, the reactions were stopped by the addition of 2 μ l of 0.2M EDTA pH 8.0. Reactions were then supplemented by the addition of 2 μ l yeast tRNA (10mg/ml) and DEPC-dH₂O to a final volume of 50 μ l. Probes were then purified by phenol:chloroform:isoamyl alcohol (25:24:1) extraction and reprecipitated on ice a total of three times using NH₄⁺CH₃COO⁻/95% EtOH and resuspended in a final volume of 50 μ l DEPC-dH₂O. One-tenth of probe volume was used after the final resuspension for scintillation counting.

Hybridization

Slides were removed from storage at -80°C and allowed to slowly warm to RT in a sealed slide box containing desiccant and then placed on a 37°C slide-warmer for 15min. The sections were then rinsed in 1x PBS for 1min followed by a Proteinase K treatment for 8min at 37°C (Proteinase K ($5\mu\text{g}/\text{ml}$) (Sigma) in 0.1M Tris-Cl pH 8.0, 50mM EDTA pH 8.0). After Proteinase K treatment, sections were rinsed twice in 1x PBS and then dipped in 0.1M Triethanolamine (TEA) pH 8.0 for 3min. Next, tissue was acetylated by treatment with 0.1M TEA/0.3% acetic anhydride for 20min at RT. After acetylation, sections were rinsed twice in 2xSSC and dehydrated in ascending alcohols. Slides were then dried under vacuum for ≥ 2 hrs at RT.

After desiccation, slides were placed on a 55°C slide-warmer and sections were completely covered with 200-300 μl of pre-hybridization solution (2x Hybridization: 1.2M NaCl, .40mM Tris-Cl pH 7.5, 8x Denhardt's solution (Sigma), 2mM EDTA, 20mM DTT, 2% Glycine; made with RNase-free reagents and diluted to 1x with deionized formamide before use). Pre-hybridization was allowed to continue at 55°C for 1.5hrs on a sealed slide-warmer. A moist environment was maintained by the presence of small containers of 4xSSC/50% formamide.

Prior to hybridization, a sufficient volume of 1x hybridization solution was supplemented with dextran sulfate (Sigma) at a final concentration of 200mg/ml. The 1x hybridization/dextran sulfate mixture was heated to 55°C with rotation to facilitate mixing. Just prior to hybridization, RNA probes were denatured by heating to 80°C

for 10min followed by quick chilling on ice. The denatured probes were then added at a final concentration of $\approx 1,000,000$ cpm/ml to an appropriate amount of 1x hybridization solution (100 μ l/slide) and briefly vortexed. Slides were then removed from the warmer in turn, drained of pre-hybridization solution and coverslipped with 100 μ l of 1x hybridization solution containing the appropriate probe. After all slides had been coverslipped, they were sealed with DPX mounting media (BDH Laboratory Supplies) and incubated at 55°C for 16-18hrs.

Washing Sequence/RNase Treatment

After hybridization, slides were allowed to slowly come to RT, and DPX seals were carefully removed with forceps. Coverslips were removed by soaking without agitation in 4xSSC for 20 min at RT. Slides were then treated with RNase (Type X-A, Sigma) for 1hr at 37°C (RNase buffer: 0.5M NaCl, 10mM Tris-Cl pH 8.0, 1mM EDTA). After RNase treatment, slides were subjected to the following wash sequence:

2xSSC, 1mM DTT	10min @ RT	2x
1xSSC, 1mM DTT	20min @ RT	
0.5xSSC, 1mM DTT	20min @ RT	
0.1xSSC, 1mM DTT	10min @ 68°C	3x
0.1xSSC, 1mM DTT	1min @ RT	

Upon completion of the wash sequence, slides were dehydrated in ascending alcohols (50%, 70%, 95%, 100%, 100%) and then air dried at RT (50% and 70% EtOH solutions were supplemented with 300mM $\text{NH}_4^+\text{CH}_3\text{COO}^-$ and 1mM DTT).

After drying slides were directly apposed to Biomax XAR film for 5-7 days.

Emulsions

If results of apposition to film were favorable, slides were dipped in NTB2 photographic emulsion (Kodak) diluted 1:1 with 600mM $\text{NH}_4^+\text{CH}_3\text{COO}^-$ and exposed for 15-21days at 4°C. Emulsion coated slides were developed with Kodak D-19 developer diluted 1:1 with dH_2O and Kodak fixer. Slides were then allowed to dry at RT for 2hrs. When dry, excess emulsion was removed, sections were counter-stained with 1% Neutral Red and coverslipped with DPX mounting media.

Microscopy and Image Analysis

After mounting, sections were viewed using an Olympus model BH2-RFCA microscope equipped with DApoPlan objective optics. Image analysis was carried out using the NIH Image 1.60/PPC software package on an Apple Macintosh PowerPC. Statistical operations were performed using the GB-Stat/PPC™ software package. Image preparation and construction of figures were accomplished using Adobe Illustrator 7.0™ and Adobe Photoshop 5.0™

Results

Cloning of Partial cDNAs encoding *Apteronotus* NMDAR Subunits

Screening of the Dano 1/2 and Dano 2/10 cDNA Libraries

Initial screens of the Dano 1/2 library were carried out at low stringency and yielded a number of clones, which coded for various members of the *Apteronotus* NMDAR2 subunit family. After being isolated, initial primary sequence data was obtained from the ends of clones. Clones that displayed homology to mammalian NMDAR2 cDNAs on at least one end (based on NCBI BLAST database searches) were sequenced in their entirety from both strands.

It was determined that Clone 4 (1422bp) and Clone 13 (1481bp) could be assembled into one contig which corresponded to a single open reading frame (ORF) of 1692bp. This contig was found to show a high degree of homology to amino acids 431-995 (>81% identity) of the mammalian NMDAR2 protein and was therefore assigned the putative identity of Apt. NMDAR2B (Figure 6).

In the same manner, it was determined that Clones 8.2 (1522bp) and 25 (895bp) could be assembled into a single contiguity with an ORF of 1842bp which displayed a high degree of homology to the mammalian NMDAR2C protein. In the case of this cDNA however, it was found that the coding sequence corresponding to the region from M1 to M4 bore a much higher degree of homology to its mammalian counterpart (83% identity) than did regions 5' of M1 or 3' of M4 (39% and 50% identities respectively). To verify that the

divergent 3' end of this cDNA was in fact part of the Apt. NMDAR2C coding sequence, an RNase protection assay was performed using a probe incorporating both conserved and divergent regions. This experiment indicated that the conserved region spanning M1-M4 and the divergent 3' end of this clone were part of the same transcript (data not shown). Based on this homology, it was assigned the putative identity of Apt. NMDAR2C (Figure 7).

In the case of NMDAR2D, a single clone (Clone 25) of 1119bp was isolated, which was found to bear a high degree of homology to its mammalian counterpart. This clone was found to yield a single continuous ORF that corresponded to amino acids 620-933 (78% identity) of the *R. norvegicus* NMDAR2D protein and was given the putative identity of Apt. NMDAR2D (Figure 8). Please see Figure 5 for a graphical representation of clones obtained.

Figure 5: Graphical Representation of Isolated Apt.NMDAR2 cDNAs.

Schematic representation of isolated Apt. NMDAR2 cDNAs. Solid black bars indicate regions of homology. Amino acid residues are numbered according to published protein sequence of *R. norvegicus* NMDAR2 subunits. Coding regions of isolated clones are indicated by grey bars bearing the clone's designation. Diagram is not drawn to scale.

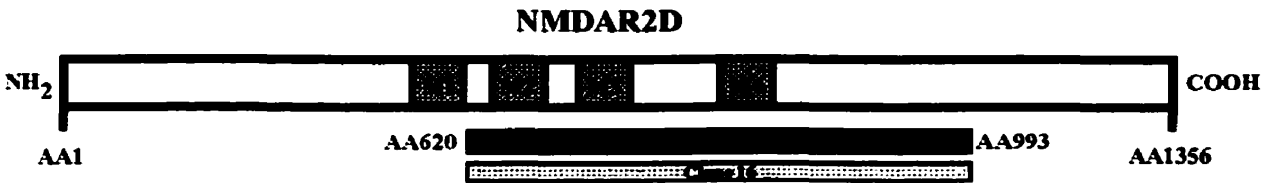
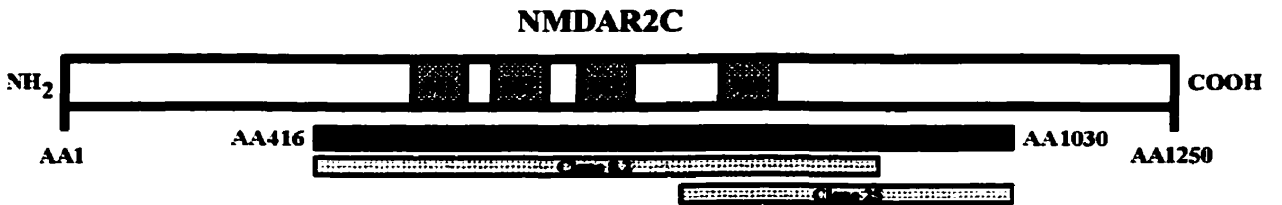
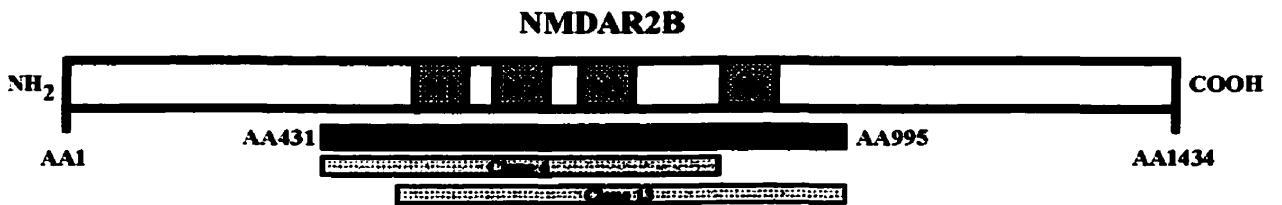
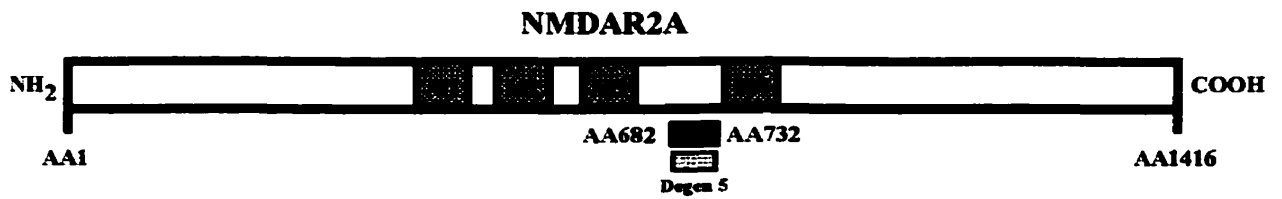


Figure 6: Nucleotide and Protein Comparisons, Apt. NMDAR2B.

Clustal protein alignment of Apt. NMDAR2B vs. published sequences for *R. norvegicus* NMDAR2B and *M. musculus* Epsilon 2 sequences. Shading indicates residues matching the consensus. Regions corresponding to NMDAR2 transmembrane domains are indicated by segments labeled M1, M3, and M4. Re-entrant loop region is indicated as M2.

1 MR-----I S E Q G D S G V R
425 L S G T C M R N I S E Q G D S G V R
425 -----I S E Q G D S G V R
Apt NMDAR2B Pro
Rat NMDAR2B Pro
Mouse Epsilon 2 Pro

24 A V
465
449
Apt NMDAR2B Pro
Rat NMDAR2B Pro
Mouse Epsilon 2 Pro

64 N H I
505
489
Apt NMDAR2B Pro
Rat NMDAR2B Pro
Mouse Epsilon 2 Pro

M 1
104 L I L
545
529
Apt NMDAR2B Pro
Rat NMDAR2B Pro
Mouse Epsilon 2 Pro

M 2
144 T A R
585
569
Apt NMDAR2B Pro
Rat NMDAR2B Pro
Mouse Epsilon 2 Pro

M 3
184
625
609
Apt NMDAR2B Pro
Rat NMDAR2B Pro
Mouse Epsilon 2 Pro

224 R S
665
649
Apt NMDAR2B Pro
Rat NMDAR2B Pro
Mouse Epsilon 2 Pro

264 V H N E Q A M
705
689
Apt NMDAR2B Pro
Rat NMDAR2B Pro
Mouse Epsilon 2 Pro

304 H
745
729
Apt NMDAR2B Pro
Rat NMDAR2B Pro
Mouse Epsilon 2 Pro

344 H V
785
769
Apt NMDAR2B Pro
Rat NMDAR2B Pro
Mouse Epsilon 2 Pro

M 4
384 L A L T V L L H L T T
825
809
Apt NMDAR2B Pro
Rat NMDAR2B Pro
Mouse Epsilon 2 Pro

424 E V E D K T A L L R Q H D P H T Q H P A
865
849
Apt NMDAR2B Pro
Rat NMDAR2B Pro
Mouse Epsilon 2 Pro

460 S H G G D A A L
902
886
Apt NMDAR2B Pro
Rat NMDAR2B Pro
Mouse Epsilon 2 Pro

500 A - - T D A P P A F P D D M K H L
942
926
Apt NMDAR2B Pro
Rat NMDAR2B Pro
Mouse Epsilon 2 Pro

538 E Q F L P R A E F A R L E
982
966 P H S I G S T S S I D G L Y D C
Apt NMDAR2B Pro
Rat NMDAR2B Pro
Mouse Epsilon 2 Pro

Figure 7: Nucleotide and Protein Comparisons, Apt. NMDAR2C.

Clustal protein alignment of Apt. NMDAR2C vs. published sequences for *R. norvegicus* NMDAR2C and *M. musculus* Epsilon 3 sequences. Shading indicates residues matching the consensus. Regions corresponding to NMDAR2 transmembrane domains are indicated by segments labeled M1, M3, and M4. Re-entrant loop region is indicated as M2.

Figure 8: Nucleotide and Protein Comparisons, Apt. NMDAR2D.

Clustal protein alignment of Apt. NMDAR2D vs. published sequences for *R. norvegicus* NMDAR2D and *M. musculus* Epsilon 4 sequences. Shading indicates residues matching the consensus. Regions corresponding to NMDAR2 transmembrane domains are indicated by segments labeled M3, and M4. Re-entrant loop region is indicated as M2.

1 H ----- E P V I Apt NMDAR2D Pro
 600 [redacted] Rat NMDAR2D Pro
 600 [redacted] A Mouse Epsilon 4 Pro

M 2

21 I K Apt NMDAR2D Pro
 640 [redacted] Rat NMDAR2D Pro
 640 [redacted] Mouse Epsilon 4 Pro

M 3

61 Q I K K H F R R Apt NMDAR2D Pro
 680 [redacted] Rat NMDAR2D Pro
 680 [redacted] Mouse Epsilon 4 Pro

101 T H T Q I O P E S G R G P Q S O N R V Apt NMDAR2D Pro
 720 [redacted] Rat NMDAR2D Pro
 720 [redacted] Mouse Epsilon 4 Pro

141 G Q D Apt NMDAR2D Pro
 759 [redacted] Rat NMDAR2D Pro
 759 [redacted] Mouse Epsilon 4 Pro

181 G D T Q S W K T V Q E N Apt NMDAR2D Pro
 799 [redacted] Rat NMDAR2D Pro
 799 [redacted] Mouse Epsilon 4 Pro

221 I L K S M H K S Apt NMDAR2D Pro
 838 [redacted] Rat NMDAR2D Pro
 838 [redacted] Mouse Epsilon 4 Pro

M 4

261 E N L I I F N G V E D ----- Apt NMDAR2D Pro
 878 [redacted] Rat NMDAR2D Pro
 878 [redacted] Mouse Epsilon 4 Pro

283 - V G S G S I Q N D I T T N Y Q N M L K M L Q T A K D I V S S K V E - Apt NMDAR2D Pro
 918 [redacted] I Rat NMDAR2D Pro
 918 [redacted] L Mouse Epsilon 4 Pro

321 ----- N S D N A T K T I E H W S R Q ----- G Q S A S P H T G Apt NMDAR2D Pro
 958 [redacted] D Rat NMDAR2D Pro
 958 [redacted] E Mouse Epsilon 4 Pro

348 D H H Apt NMDAR2D Pro
 998 [redacted] Rat NMDAR2D Pro
 998 [redacted] Mouse Epsilon 4 Pro

Isolation of a Fragment Homologous to NMDAR2A by Degenerate PCR

Screens of the Dano 1/2 and Dano 2/10 libraries failed to produce any clones which displayed obvious homology to the mammalian NMDAR2A cDNA; the reason for this failure remains unclear but is thought to involve low message abundance. Therefore, an approach that utilized degenerate PCR was employed to isolate a fragment of the apteronotid NMDAR2A cDNA.

Amplification using degenerate primers corresponding to regions amino acids 667-673 and 712-718 of the published *R. norvegicus* NMDAR2B protein sequence was carried out (see Methods) and a DNA fragment of the expected size (≈ 154 bp) was obtained. After gel purification, the fragment was subcloned in to pGEM-T (Promega) and a large number of transformants were obtained. Primary sequence data was obtained from a total of 50 of these clones and a novel sequence of 154bp in length (Degen 5) was discovered which displayed a high degree of homology (86% amino acid identity) to the *R. norvegicus* NMDAR2A cDNA. In addition, sequence comparisons of this fragment with corresponding regions of Apt. NMDAR2B, C and D clones support the conclusion that it is indeed a novel sequence (Figure 9). During the course of transformant screening, the Degen 5 sequence was isolated a total of 8 times in addition to fragments corresponding to previously isolated *Apteronotus* NMDAR2B and NMDAR2C clones.

Figure 9: Nucleotide and Protein Comparisons, Degen 5 vs. Apt. NMDAR2B/C/D.

Clustal nucleotide and protein alignments of Apt. NMDAR2A fragment (Degen 5) vs corresponding regions of Apt. NMDAR2B, Apt. NMDAR2C, and Apt. NMDAR2D. **A**, Clustal protein alignment. **B**, Clustal nucleotide alignment.

In situ Hybridization

In situ hybridization experiments revealed that the distribution of NMDAR2 mRNAs within the brain of *A. leptorhynchus* is complex and surprisingly discrete. Hybridization patterns were generally found complementary to those described for Apt. NMDAR1 mRNA by Bottai et al. (1997, 1998). However upon closer investigation, it was found that the distribution of Apt. NMDAR2 mRNAs (particularly in the ELL) is regulated in a cell specific manner.

Apt. NMDAR2 mRNA Expression in Forebrain Regions

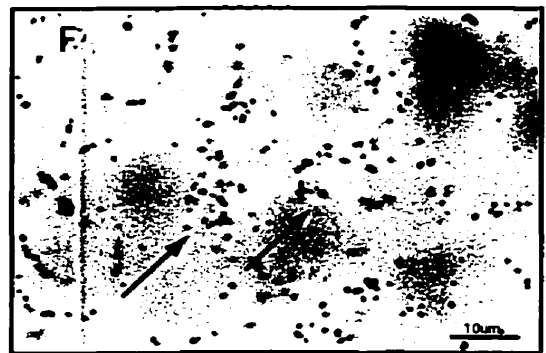
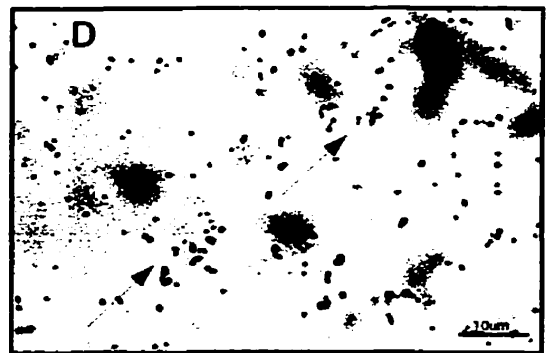
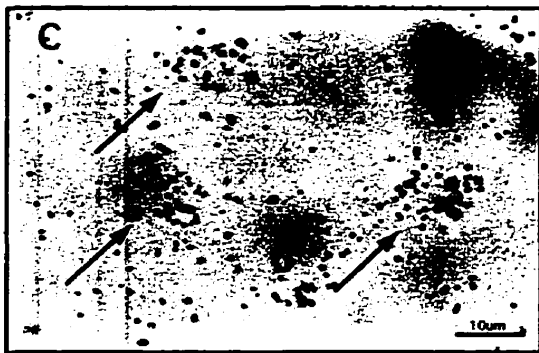
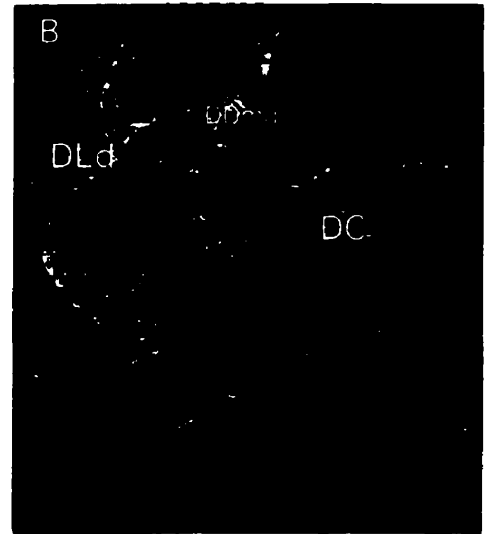
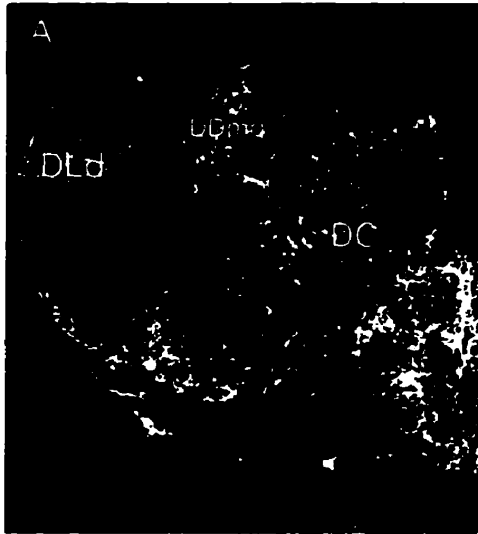
Expression was detected for both Apt. NMDAR2A and Apt. NMDAR2B messages in forebrain regions. Modest levels of Apt. NMDAR2A message were detected in cells of the central division of the dorsal forebrain (DC), dorsal subdivision of the dorsolateral telencephalon (DLd), and the magnocellular subdivision of the dorsal division of the dorsal forebrain (DDmg) (Figure 10).

Apt. NMDAR2B mRNA was detected in DC, DLd, and DDmg as well as several ventral forebrain cell groups. Levels of Apt. NMDAR2B mRNA expression appeared to be slightly higher than those of Apt. NMDAR2A in DC and DLd (Figure 10) but comparable in cells of DDmg (data not shown).

The expression of Apt. NMDAR2C mRNA in forebrain regions was confined to one discrete cell group, the ventral subdivision of the ventral telencephalon (Vv). No evidence for the expression of

Figure 10: Expression of Apt. NMDAR2A and Apt. NMDAR2B mRNAs in Forebrain.

Expression patterns of Apt. NMDAR2A and Apt. NMDAR2B mRNAs in the forebrain of *A. leptorhynchus* as revealed by *in situ* hybridization. **A**, Dark-field micrograph of Apt. NMDAR2B expression patterns in forebrain. Note intense labeling of cells in the central division of the dorsal forebrain (DC), dorsal subdivision of the dorsolateral telencephalon (DLd), and magnocellular subdivision of the dorsal division of the dorsal forebrain (DDmg). **B**, Expression of Apt. NMDAR2A mRNA in identical regions of the forebrain. As with Apt. NMDAR2B, labeling can be detected in DC, DLd and DDmg. However, the cells of DC and DLd do not show as intense a signal; labeling of DDmg is comparable. **C**, High-power light micrograph of cells in DC labeled with Apt. NMDAR2B probe. **D**, Three cells of the DC are also shown to show labeling with Apt. NMDAR2A probe, but to a lesser extent. **E**, Apt. NMDAR2B hybridization pattern within DLd. **F**, Cells of this region are also shown to label to a similar extent with the Apt. NMDAR2A probe.



Apt. NMDAR2D mRNA was detected in forebrain regions (data not shown).

Detection of Apt. NMDAR2A and Apt. NMDAR2B mRNA expression in DC, DLd and DDmg concur with the findings of Bottai et al. (1997, 1998) who reported high levels of Apt. NMDAR1 message in these regions. These overlapping expression patterns suggest that functional NMDAR complexes are present in these apteronotid forebrain structures. Because the function of specific cell types within the forebrain circuitry of *A. leptorhynchus* is presently unknown, specific conclusions as to the exact role played by NMDAR complexes in this region are not possible.

Apt. NMDAR2 mRNA Expression in Midbrain Regions

Expression of Apt. NMDAR2A mRNA in the midbrain was low and very diffuse. Signal levels rarely rose above background in these regions, making identification of discrete expression patterns almost impossible.

Apt. NMDAR2B mRNA was found to be expressed in the midbrain in a pattern almost identical to that of Apt. NMDAR1 (Bottai et al., 1997; Bottai et al., 1998). Expression of Apt. NMDAR2B mRNA was found to be identical to that of Apt. NMDAR1 in regions associated with the descending control of the electrosensory system such as the dorsal torus semicircularis (TSd), optic tectum (TeO), and nucleus praeminentialis dorsalis (nPD). The observation of Apt. NMDAR2B mRNA in the nPD is of particular interest as it coincides with the findings of Bottai et al. (1997) and reinforces the idea that

NMDA-mediated transmission is involved in the descending attentional control of electroreception (Berman et al., 1997).

Expression of the Apt. NMDAR2C mRNA was found to be restricted to cerebellar structures such as the corpus cerebelli (CCb) and valvula cerebelli pars lateralis (VCbl). This finding is in close agreement with similar studies carried out in mammalian systems which report significant restriction of NMDAR2C message to cerebellar structures (Monyer et al., 1994; Wanatabe et al., 1992; Wanatabe, M. et al., 1994).

Apt. NMDAR2D mRNA expression was not detectable in the vast majority of midbrain structures. The sole exception was a structure known as the torus longitudinalis (TL) whose exact function in the apteronotid brain is unknown (L. Maler, personal communication).

Apt. NMDAR2 mRNA Expression in the ELL

All Apt. NMDAR2 mRNAs were found to be expressed at relatively high levels within regions of the ELL. Patterns of hybridization were markedly different for all messages.

At the level of the dorsal ELL, Apt. NMDAR2A message was detected at low levels within the eminentia granularis pars posterior (EGp) (Figure 11A) and at significantly higher levels in Purkinje cells (Figure 11G). The detection of Apt. NMDAR2A message in the EGp is of significance because this cerebellar region is the origin of a series of parallel fibre networks that extend into the dorsal molecular layer (DML) of the ELL. This parallel fibre network is known to make synaptic contacts upon the apical dendrites of ELL pyramidal cells and is postulated to be part of a sensory gain control

mechanism (Bastian, J. 1986; Bastian and Courtright, 1991; Bastian, J. 1995). The observation of Apt. NMDAR2A mRNA expression in Purkinje cells is mysterious in light of the findings of Bottai et al. (1997) who reported no detection of Apt. NMDAR1 message in these cells.

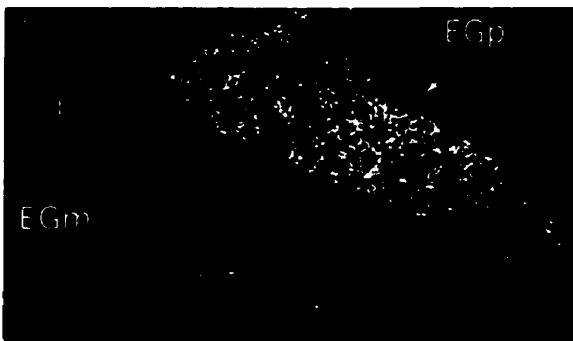
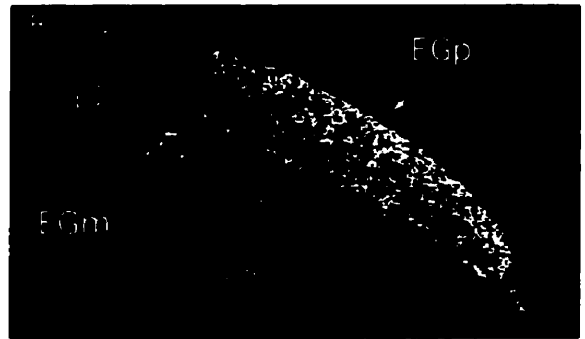
Hybridization of the Apt. NMDAR2B probe was detected in EGp, and at low levels in some cells of the eminentia granularis pars medialis (EGm) (Figure 11B). This message was also detected at relatively high levels in Purkinje cells (Figure 11H). Expression of the Apt. NMDAR2C mRNA was confined to the granule cells of EGp and was not detected in EGm or Purkinje cells (Figure 11C).

Apt. NMDAR2D message was found to be present in cells of the EGm at very high levels and is clearly visible in cells migrating from this region to EGp. This finding is particularly interesting in light of findings that the EGm is a proliferative zone within the apteronotid brain, constantly producing new cells throughout the life of the animal (Zupanc, G. K. and Horschke, I., 1995; Zupanc, G. K. and Zupanc, M. M., 1992b). No Apt. NMDAR2D message was found to be present in Purkinje cells (Figure 11D). Comparison to expression patterns of Apt. NMDAR1 (Figure 11E) (Bottai et al., 1997) illustrates that Apt. NMDAR2 mRNAs are found in all regions where Apt. NMDAR1 message is detected (EGp, EGm, migrating granule cells from EGm). A notable peculiarity is the observation of Apt. NMDAR2A/B mRNA expression in Purkinje cells in the absence of detectable levels of Apt. NMDAR1 message (Bottai et al., 1997; Bottai et al., 1998).

Previous studies have indicated that Apt. NMDAR1 mRNA is expressed at very high levels in specific areas of the ventral ELL; including the entire depth of the pyramidal and granule cell layers of

Figure 11: Expression of Apt. NMDAR2 Subunit mRNAs in Dorsal ELL.

Comparison of Apt. NMDAR2 mRNA expression patterns in the dorsal electrosensory lateral line lobe (ELL). **A**, Low-power dark-field micrograph of Apt. NMDAR2A mRNA expression patterns. Weak labeling can be detected in cells of the eminentia granularis pars posterior (EGp). **B**, Expression pattern of Apt. NMDAR2B mRNA is typified by moderate labeling of EGp cells, very intense labeling of Purkinje cells in the corpus cerebelli (CCb), and very low expression within some cells of the eminentia granularis pars medialis (EGm). **C**, Apt. NMDAR2C message appears to be restricted to cells of the EGp. **D**, Cells of the EGp display labeling with the Apt. NMDAR2D probe. Very intense labeling is seen in the cells of EGm, and expression of this mRNA can be detected in cells migrating from EGm towards EGp. **E**, Expression pattern of Apt. NMDAR1 mRNA. This message can be seen to co-localize with those of the various Apt. NMDAR2 subunits. Of interest is the fact that no Apt. NMDAR1 message can be detected in cerebellar Purkinje cells. **F**, Negative control. Hybridization using a sense Apt. NMDAR2C probe. **G**, High-power light micrograph of cerebellar Purkinje cell showing positive hybridization with Apt. NMDAR2A probe. **H**, Purkinje cells labeled with the Apt. NMDAR2B probe.



all four topographically organized segments (MS, CMS, CLS, and LS) (Figure 12E). Apt. NMDAR2A mRNA was detected at consistently high levels throughout the depth of the pyramidal cell layer (PCL) and somewhat lower levels in granule cells across all segments (Figure 12A). Apt. NMDAR2B mRNA was detected in moderate levels in granule cells across segments, but in contrast to Apt. NMDAR2A, it was found to be restricted to only the most dorsal pyramids of the PCL (Figure 12A, 12B). This difference was quantified by comparing grain densities in dorsal pyramids to those located in the ventral PCL. This finding is interesting in light of previous studies which have described differences between dorsally and ventrally positioned pyramidal cells in terms of morphology (Bastian, 1991) and protein expression (Berman, N. J. et al., 1995; Zupanc, G. K. H. et al., 1992a). Figure 13 illustrates the differences in labeling seen with Apt. NMDAR2B as compared to Apt. NMDAR1 which is known to be expressed throughout the PCL (Figure 13A, 13B). Figure 13C illustrates labeling of a dorsal pyramidal cell with the Apt. NMDAR2B probe, while Figure 13D indicates an example of a ventral pyramid expressing Apt. NMDAR1 mRNA. After data analysis it was found that a highly significant difference in grain density exists between dorsal and ventral cells of the PCL labeled with the Apt. NMDAR2B probe (dorsal mean=17.8, ventral mean =10.3, unpaired t-test, $t(\text{two-tailed})=10.3$, $p<0.0001$) (Figure 12F). In addition, it was found that dorsal pyramids of the LS had a lower grain density than those of the remaining three segments (one-way ANOVA, $F(3,56)=4.63$, $p<0.005$; Bonferroni post-hoc comparison $p<0.01$) (Figure 13E).

Figure 12: Expression of Apt. NMDAR2 Subunit mRNAs in Ventral ELL.

Comparison of Apt. NMDAR subunit mRNA expression pattern within the ventral ELL. **A**, Expression of Apt. NMDAR2A mRNA. Labeling is detectable throughout the depth of the pyramidal cell layer (PCL) and across all segments. Low levels of expression can also be detected throughout the granule cell layer (GCL). **B**, Expression pattern of Apt. NMDAR2B mRNA. Differential labeling of cells throughout the dorso-ventral aspect of the PCL cannot be detected at this magnification, but it is evident that cells of the lateral segment (LS) hybridize less strongly than those of the more medial segments. **C**, Expression of the Apt. NMDAR2C mRNA labeling can be seen throughout the PCL and GCL of medial segment (MS), centromedial segment (CMS), and centrolateral segment (CLS), but is absent from cells of the LS. **D**, Expression of the Apt. NMDAR2D message cannot be detected in pyramidal cells of any segment. Strong hybridization signals can be seen in the granule cells of the CMS but noticeably decline in CLS and LS. **E**, Expression of the Apt. NMDAR1 mRNA is intensive throughout the PCL and GCL of all segments. **F**, Schematic indicating relative positions of PCL and GCL in field.

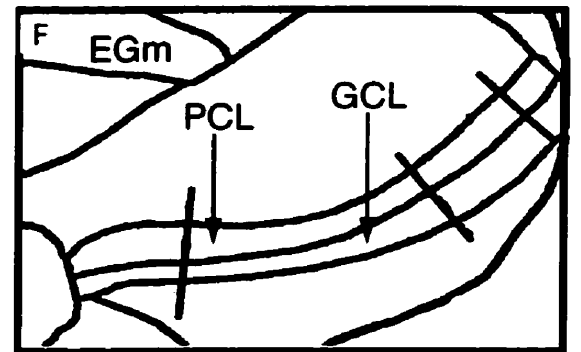
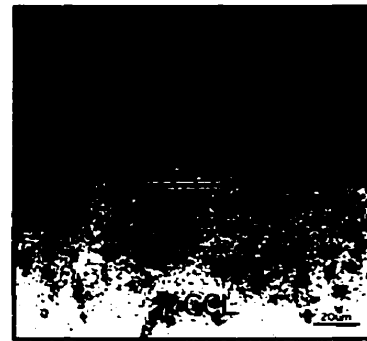
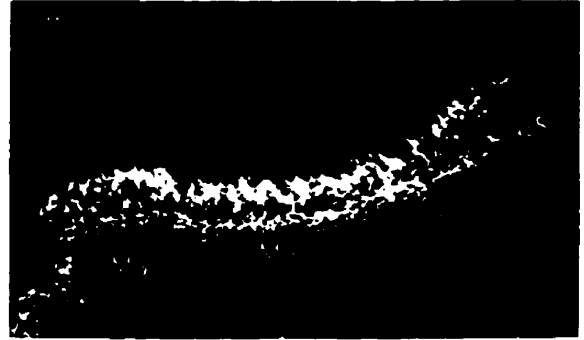


Figure 13: Expression of Apt. NMDAR2B mRNA in Pyramidal Cell Layer.

Differential expression of Apt. NMDAR2B mRNA in the PCL as a function of dorso-ventral positioning. **A**, Expression of Apt. NMDAR2B message is confined to dorsal pyramidal cells. **B**, An adjacent section from the same brain probed for Apt. NMDAR1 message displaying signal throughout the depth of the PCL. Note the obvious difference in labeling intensity of cells in the PCL of the LS. **C**, Light micrograph indicating the position of a dorsally positioned cell within the PCL. **D**, Hybridization pattern of cells probed for Apt. NMDAR1 message within the corresponding map (CMS) of an adjacent section. A typical deep pyramidal cell is indicated. **E**, Statistical summary of differences in grain density observed with Apt. NMDAR2B labeling across segments. Data was analyzed using a one-way analysis of variance (ANOVA) followed by Bonferroni *post hoc* comparison (N=sample number). **F**, Statistical summary of differences in grain density observed in Apt. NMDAR2B hybridizations as a function of dorso-ventral positioning of pyramidal cells. Statistical significance was tested using an unpaired t-test (two-tailed). Measurements are pooled across segments.



E Table 2: Segmental Differences in NR2B Grain Density

<i>Segment</i>	<i>Mean Grain Density</i>	<i>N</i>	<i>Standard Deviation</i>	<i>F_(3,56)</i>	<i>p-value</i>
MS	16.8	15	1.7	4.63	p<0.005
CMS	19.6	15	2.4		
CLS	19	15	3.8		
LS*	15.6	15	3.2		

F Table 3: NR2 Grain Density as a Function of Dorso-Ventral Position

<i>Cell Type</i>	<i>Mean Grain Density</i>	<i>N</i>	<i>t (two-tailed)</i>	<i>p-value</i>
Superficial	17.8	40	10.3	p<0.0001
Deep	10.3	30		

Apt. NMDAR2C message was found to be expressed at low levels in granule cells of all segments. Expression was detected throughout the depth of the PCL in MS, CMS, and CLS but was noticeably lower (although present) in pyramids of the LS (Figure 12C, 14A-D). This difference was quantified by comparing pooled grain densities of Apt. NMDAR2A-labeled pyramidal cells and Apt. NMDAR2C-labeled pyramidal cells across segments in adjacent sections. After analysis, it was found that pyramidal cells of the LS have significantly lower grain densities than those in other segments (one-way ANOVA, $F(3,116)=83.8$, $p<0.001$; Bonferroni post-hoc comparison, $p<0.01$) (Figure 14E). The exact reason for the effective exclusion of Apt. NMDAR2C mRNA from cells of the LS is unclear at present. Nevertheless, it is thought provoking in the sense that it illustrates clear heterogeneity of receptor complement among highly homologous cell groups.

Apt. NMDAR2D message was found to be restricted entirely to the granule cell layer (GCL) of the ventral ELL, with no detectable signal being seen in pyramidal cells of any segment. Expression of the Apt. NMDAR2D message in the GCL was found to decrease as a function of segment medial-lateral positioning. The highest levels of Apt. NMDAR2D mRNA expression were found in granule cells of the CMS, and declined steadily as segments progress laterally towards LS. Because of the difficulties inherent in measuring grain densities in small granule cells, this difference is illustrated qualitatively in Figure 15. This finding is interesting because it is a rare example of NMDAR2D mRNA being detected in the cells of a sensory apparatus.

Figure 14: Differential Expression of Apt. NMDAR2C mRNA across Segments.

Comparison of Apt. NMDAR2C mRNA expression levels across segments. **A**, Uniform expression levels of Apt. NMDAR2A mRNA can be clearly seen throughout the depth of the PCL across all segments. **B**, Hybridization of an adjacent section from the same brain with the Apt. NMDAR2C probe. Expression of this transcript can be seen throughout the depth of the PCL in MS, CMS, and CLS but is noticeably absent from pyramidal cells of the LS. **C**, Strong labeling of pyramidal cells of the LS can be seen with Apt. NMDAR2A probe. **D**, Labeling of an LS pyramidal cell from an adjacent section with the Apt. NMDAR2C probe. **E**, Summary statistics describing a significant decrease in labeling of LS pyramidal cells (as compared to those of other segments) with the Apt. NMDAR2C probe. Note the comparative homogeneity of grain densities observed across segments found in Apt. NMDAR2A hybridizations. Data analysis was carried out using one-way analysis of variance (ANOVA) followed by Bonferroni *post hoc* comparisons (N=number of cells counted, SD=standard deviation).

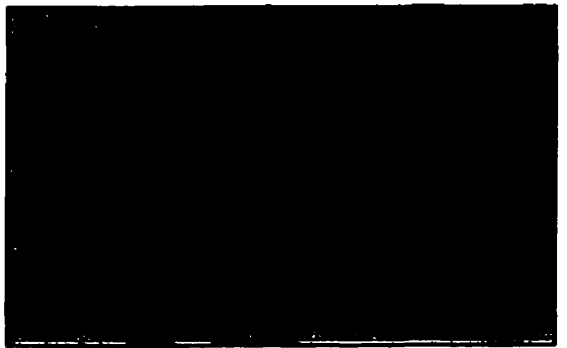
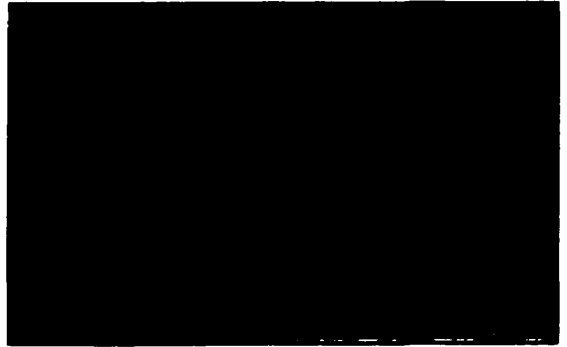


E Segmental Comparison of Grain Density, Apt. NR2A vs Apt. NR2C

<i>NMDAR2 Probe</i>	<i>Segment</i>	<i>Mean Grain Density</i>	<i>N</i>	<i>SD</i>	<i>F_(3 116)</i>	<i>p-value</i>
Apt. NR2A	MS	15.7	30	3	83.8	p<0.0001
	CMS	15.7	30	3.1		
	CLS	15.3	30	3.4		
	LS	15.6	30	2.1		
Apt. NR2C	MS	14.1	30	3.7		
	CMS	13.7	30	2.6		
	CLS	14.6	30	2.1		
	LS*	6.1	30	2.7		

Figure 15: Apt. NMDAR2D mRNA Expressed in a Gradient throughout the Granule Cell Layer.

Comparison of Apt. NMDAR2D mRNA expression in granule cells across segments. **A**, The Apt. NMDAR2D probe can be clearly seen to hybridize strongly over the granule cells of the CMS. Expression levels of Apt. NMDAR2D mRNA are seen to decline sharply in the GCLs of more lateral segments. **B**, Grains deposited over granule cells of the CMS. **C**, In the GCL of the CLS signal strength is seen to decline significantly. **D**, In the GCL of the LS, signal drops to the point of making identification of individual granule cells difficult.



Discussion

Isolation of Partial Apt. NMDAR2 subunit cDNAs

Previous work has shown that a high degree of sequence homology (>81% amino acid identity) exists between the Apt. NMDAR1 cDNA and examples of its mammalian, avian, and amphibian counterparts (Bottai et al., 1997; Bottai et al., 1998). It now appears that a similar degree of conservation may reasonably be expected in certain regions of the Apt. NMDAR2 subunit family. High levels of sequence conservation with their mammalian counterparts (>80% identity) have been described in regions spanning the three transmembrane domains and re-entrant loop (M1, M3, M4 and M2 respectively). Such high levels of sequence conservation argue for the evolutionary importance of these regions in the function of these proteins (Li, W.-H. and Graur, D., 1991). Although a high level of sequence conservation was observed throughout the length of the Apt. NMDAR2B cDNA (81% identity overall), this was not apparent in Apt. NMDAR2C or Apt. NMDAR2D. These two cDNAs display a high degree of sequence conservation in areas corresponding to membrane spanning domains but were found to diverge sharply from their mammalian counterparts in regions 3' of the fourth transmembrane domain (M4). Such divergence may prove to be of significance because of the importance of NR2 carboxy-terminal domains in NMDAR modulation, localization, and postulated involvement in intracellular signaling cascades (Ehlers et al., 1996a; Kornau et al.,

1995; Moon et al., 1994; Niethammer et al., 1996; Sprengel et al., 1998).

In the case of the Apt. NMDAR2A fragment isolated, a very high degree of sequence conservation was noted in comparison to the mammalian homologue (86% amino acid identity). The region of NMDAR2A coded for by the Apt. NMDAR2A fragment corresponds to a segment of the extracellular loop between M3 and M4; given the high degree of sequence similarity, it is not unreasonable to expect such homology to extend throughout the M1-M4 regions. However, because of the observed divergence of Apt. NMDAR2C, and Apt. NMDAR2D in regions 5' and 3' of the M1-M4 region, no speculation can be made as to the degree of conservation to be expected in the amino- and carboxy-termini of Apt. NMDAR2A.

Distribution of Apt. NMDAR2 mRNAs

In situ hybridization studies have revealed that NMDAR2 mRNAs are distributed in a complex and remarkably discrete pattern within the apteronotid brain. Globally, expression patterns of the various Apt. NMDAR2 mRNAs agree in terms of level and locale with those of their mammalian homologues (Ishii et al., 1993; Monyer et al., 1994; Wanatabe et al., 1992). In addition, Apt. NMDAR2 messages have been found to be expressed in patterns that overlap with those of Apt. NMDAR1 (Bottai et al., 1997), indicating a high probability that functional NMDARs are present in the majority of labeled cells.

Observations of Apt. NMDAR2A and Apt. NMDAR2B message expression in forebrain regions concur with results from similar mammalian studies and indicate that, as in mammals, NMDAR2A and

NMDAR2B subunits may play an important role in the organization and plasticity of cortical circuitry (Fox, K., 1995; Fox, K. et al., 1999; Quinlan et al., 1999; Williams et al., 1993). Observations of Apt. NMDAR2B and Apt. NMDAR2C mRNA expression within a region of the ventral forebrain (Vv) may be of some consequence to the understanding of the electrosensory modality. Vv has been demonstrated previously to be a region involved in a circuit which controls the modulation of electric organ discharge in the weakly electric fish *Eigenmannia virencens* (Wong, C. J. H., 1997).

Findings of Apt. NMDAR2A and Apt. NMDAR2B mRNA expression in Purkinje cells raise a number of interesting questions about the possible role of NMDARs in this cell type. In contrast to mammalian studies which report the expression of NMDAR1 subunits in this cell type with no concomitant expression of NMDAR2 subunits (Monyer et al., 1994), apteronotid Purkinje cells appear to express two NMDAR2 mRNAs (A/B) in the absence of detectable NMDAR1 message. It has been argued that mammalian Purkinje cells do not produce functional NMDAR complexes (Farrant, M. and Cull-Candy, S. G., 1991). However, other investigators report the detection of NMDA-mediated currents in Purkinje cells during certain developmental periods (Garthwaite, G. et al., 1987; Rosenmund, C. et al., 1992). How apteronotid Purkinje cell physiology compares to that of mammals in this respect remains to be elucidated.

Observations of Apt. NMDAR2 mRNA expression within the eminentia granularis pars posterior (EGp) (Figure 11) are consistent with earlier reports of NMDA binding in this brain region (Maler and Monaghan, 1991). Apt. NMDAR2C mRNA was found to be the most abundantly expressed message in this structure and this finding is in

close agreement with previous studies which show NMDAR2C to be the predominant NR2 message expressed in mature cerebellar granule cells (Audinet et al., 1994; Farrant et al., 1994; Monyer et al., 1994; Takahashi, T. et al., 1996; Wanatabe et al., 1992). In addition, it is interesting to note that although expression of NMDAR2B and NMDAR2D mRNAs are severely reduced or undetectable in most cerebellar granule cells of the mammal, these messages are expressed to a considerable degree in the apteronotid EGp. This observation may be partially explained by the fact that unlike the mammalian brain, the adult apteronotid brain continues to produce large numbers of new granule cells in the adult organism (Zupanc, G. K. H., 1999). It has been demonstrated previously in mammalian systems that cerebellar granule cells transiently express NMDAR2B mRNA while in immature, migratory phases (Audinet et al., 1994; Farrant et al., 1994; Monyer et al., 1994). It may be the case that the observed Apt. NMDAR2B mRNA expression in EGp is due to the presence of a large sub-population of migratory granule cells from EGp (see below) in the process of forming correct synaptic associations.

As previously indicated, the apteronotid CNS differs markedly from that of the mammal in the respect that maintains a number of active cell proliferation zones. In fact, it has been estimated that over any given 2 hour period up to 100,000 cells are mitotically active within the CNS of *A. leptorhynchus* (Zupanc and Horschke, 1995; Zupanc and Zupanc, 1992b). Approximately 75% of the cells produced in this manner have been found to arise from cerebellar regions, including the eminentia granularis medialis (EGm) (Zupanc and Horschke, 1995). Therefore, recalling that NMDAR2D is the

predominant NMDAR2 transcript expressed in the embryonic mammalian CNS (Monyer et al., 1994), the finding that the cells of the EGm display high levels of Apt. NMDAR2D message is of considerable interest. It would appear that in the apteronotid CNS, as in the mammal, expression of the NMDAR2D message is one of the hallmarks of early neuronal development. Cells of the EGm have been demonstrated to express Apt. NMDAR1 mRNAs (Figure 11E), so it is not unreasonable to assume that functional NMDAR complexes are being produced. This supposition is supported by the observations of Maler and Monaghan (1991) who report appreciable (abet low) levels of NMDA binding in the EGm region. In addition, close examination of Figure 11D reveals that cells expressing Apt. NMDAR2D message can be seen migrating dorsolaterally from EGm to EGp. It has been recently reported that glutamate can promote the migration of embryonic cortical neurons by binding to NMDA receptor complexes (Behar, T. N. et al., 1999). Taken together, these results suggest a scenario in which new neurons are born in the EGm, express functional NMDARs and migrate to EGp (a site of intense NMDA binding) using glutamatergic stimulation as a physiological impetus. Once in the EGp, these new cells could conceivably undergo further changes in NMDAR2 subunit expression (D→B→C) as they assume their final functional arrangement. Further investigation of this hypothesis will necessitate a close examination of the electrophysiological character of cells migrating from EGm. In addition, the effects of injection of NMDA antagonists into the molecular layer separating EGm from EGp in an attempt to disrupt normal migration patterns are a logical and necessary preliminary experiment.

Expression patterns of each of the Apt. NMDAR2 subunit mRNAs in the pyramidal cell layer (PCL) and granule cell layer (GCL) of the dorsal ELL have proven to be both unique and remarkably discrete. As is the case in the mammalian CNS, mRNAs encoding NMDAR2A and NMDAR2B subunits have been found to be localized to distinct sub-populations of pyramidal and granule cells (Monyer et al., 1994; Niedzielski, A. S. and Wenthold, R. J., 1995).

Upon initial inspection, levels and distribution patterns of Apt. NMDAR2A mRNA in the PCL and GCL appear to be closely matched to those of Apt. NMDAR1 (Figure 12A, 12E). The transcript is present throughout the depth of the PCL and GCL across all segments and has been detected extending into the apical dendrites of individual pyramidal cells (Figure 14C). However, closer analysis reveals that while levels of Apt. NMDAR1 transcript are known to decrease in pyramidal cells of the lateral segment (LS) (Bottai et al., 1997), expression of Apt. NMDAR2A transcript is effectively constant across segments (Figure 14E).

It is possible that decreased levels of Apt. NMDAR1 mRNA relative to Apt. NMDAR2A message in the LS may have an impact upon the number of NMDAR complexes incorporating the NR2A subunit produced in these cells. A recent study has shown that NMDARs incorporating the NR2A subunit have an open probability (P_o) \approx 3-5 fold greater than complexes which do not (Chen, N. et al., 1999). Consequently, it has been hypothesized that close regulation of NMDAR1/NMDA2A receptor complex expression may be employed in certain neural networks as a means of fine-tuning response characteristics of important cell types. Such fine-tuning may be of

vital importance to the performance of feature extraction tasks carried out by the pyramidal cells of the LS.

An excellent example of cell-specific NMDAR mRNA expression is illustrated in the case of the Apt. NMDAR2B transcript. Expression patterns of Apt. NMDAR2B mRNA were found to closely resemble those of Apt. NMDAR1. Message was detected in pyramidal and granule cells of all segments with those of the LS exhibiting the lowest degree of expression (Figure 13E). There is surprisingly close agreement between the amount of decline noted in Apt. NMDAR1 mRNA expression in pyramidal cells of the LS (15%) (Bottai et al., 1997) and that seen with Apt. NMDAR2B message (18%) (Figure 13E). At present, the functional significance of this finding is unclear.

Anatomical studies of the PCL have shown that its constituent cells are organized in a single lamina approximately 3-4 cells deep (Saunders and Bastian, 1984; Shumway, 1989b). Previous studies have demonstrated that the response characteristics of pyramidal cells vary according to the segment in which they are found and their location within the dorso-ventral aspect of the PCL (Bastian, J. and Courtright, J., 1991; Shumway, 1989a). The work of Bastian and Courtright (1991) has demonstrated that both the morphology of a pyramidal cell's apical dendritic arbor and its physiological adaptation rate can be directly correlated with its position within the pyramidal cell layer. These investigations revealed that cells positioned in the most dorsal aspect of the PCL have extensive dendritic arbors which project well into the DML (an established site of NMDA-mediated transmission (Berman et al., 1997)) and display phasic response characteristics. In contrast, cells positioned deep in the PCL were found to have much smaller dendritic arbors and

display a more tonic response profile. Subsequent work has identified additional differences in superficial and deep pyramidal cells with respect to the expression of both Inositol 1,4,5-triphosphate receptors and ryanodine binding proteins (Berman et al., 1995; Zupanc et al., 1992a). It was found that while superficial pyramidal cells possessed appreciable amounts of both proteins, deep pyramidal cells expressed very little or none. Since both of these proteins are known to be involved in the mobilization of internal calcium stores, their presence or absence may have profound effects on any number of calcium dependent signaling cascades. The present finding that expression of NMDAR1/NMDAR2B complexes may also be limited to superficial pyramidal cells adds another layer of complexity to the functional organization of the ELL. It is possible that the cell-specific co-expression of NMDAR1/NMDAR2B receptor complexes and calcium mobilizing proteins results in the establishment of a specific response profile necessary for optimal performance of the feature extraction tasks performed by these cells.

Apt. NMDAR2C mRNA was found to display a discrete pattern of expression within the ventral ELL. This transcript was localized to cells throughout the PCL and GCL of the medial, centromedial, and centrolateral segments (MS, CMS, and CLS respectively) but was found to be almost totally absent from cells of the LS.

The degree of tuberous afferent convergence upon pyramidal cells is known to vary as a function of segment. Pyramidal cells located in the LS are postulated to receive ≈ 3 times the number of receptor afferent contacts of those situated in the CMS. The result of this adaptation is that cells of the LS are found to respond to

sensory input with short latencies and possess large receptive fields with weak inhibitory surrounds. Such response characteristics are thought to predispose pyramidal cells of the LS to the efficient extraction of temporal information (Shumway, 1989b). One of the hallmark characteristics of NMDAR complexes is their sensitivity to voltage-dependent blockade by Mg^{+2} (Hollmann and Heinemann, 1994). Under physiological conditions ($\approx 1\text{mM } Mg^{+2}$), postsynaptic membranes must be depolarized by preceding or coincident inputs if the Mg^{+2} blockade is to be relieved and permit maximal NMDA-mediated transmission. However, if postsynaptic NMDAR complexes incorporate the NMDAR2C subunit, susceptibility to blockade by Mg^{+2} is greatly reduced (Ishii et al., 1993; Kutsuwada et al., 1992). It is logical to hypothesize that in the case of LS pyramidal cells, the high degree of input convergence increases the probability of coincident input, and therefore relief from Mg^{+2} blockade. If this were the case, the result would be a kind of "temporally sensitized" NMDA-mediated transmission. Any further degree of "voltage-insensitivity" of NMDA currents that might result from incorporation of NMDAR2C subunits at such synapses may prove to be detrimental to feature extraction in this particular subdivision of the ELL's neural network.

The final expression pattern to be considered is that of Apt. NMDAR2D mRNA in the ventral ELL. Compared to the previously discussed Apt. NMDAR2 mRNAs, expression of the Apt. NMDAR2D message was found to be the most restricted. No indication of this transcript could be detected in the PCL of any segment, and its expression in the GCL appeared to be constrained in a segment-

dependent manner. Evidence of Apt. NMDAR2D message could be found in the GCLs of the CMS, CLS, and LS. However, the intensity of labeling was found to steadily decrease, as segments became more lateral. Unambiguous labeling of individual granule cells was evident in the GCL of the CMS (Figure 15B), but in the LS hybridization signals had decreased to the point of making identification of individual cells difficult.

Speculation concerning the possible function of a differential distribution of Apt. NMDAR2 mRNA among sub-populations of granule cells is difficult; at present, the physiology of the ELL's GCL is largely unknown. In addition, because of their low abundance in the adult mammalian brain, small current flux, and excessively slow kinetics NMDAR2D-containing receptor complexes have not been the subjects of intense study. However, previous studies have demonstrated that NMDAR2D mRNA can be found in distinct sub-populations of cells within the adult mammalian CNS (Monyer et al., 1994).

By carefully considering the nature of the expression gradient and characteristics of the NMDAR2D protein, at least one possible explanation becomes evident. As previously discussed, pyramidal cells of the LS have been shown to have short response latencies and large receptive fields with weak inhibitory surrounds. These specializations allow the cells of the LS to act as faithful relays of temporal information. In contrast, pyramidal cells of the CMS have been shown to display comparatively longer response latencies and possess small receptive fields with strong inhibitory surrounds. Adaptations of this kind should, in theory, equip the pyramidal cells of the CMS to act as faithful relays of spatial information. (Metzner

and Juranek, 1997; Metzner, W. et al., 1998; Shumway, 1989b; Shumway, 1989a). In this sensory system, the establishment of receptive field inhibitory surrounds is dependent upon the suppression of non-basilar pyramidal cell (NBP) activity by sensory input via disynaptic contacts with inhibitory granule cells (Figure 3) (Saunders and Bastian, 1984). NMDAR complexes which incorporate the NMDAR2D subunit are known to display very long activation and deactivation time courses in addition to a lessened sensitivity to Mg^{+2} blockade (McBain and Mayer, 1994). Therefore, if these subunits were incorporated in the NMDAR complexes of granule cells they may serve to "prime" NMDA-mediated transmission by fluxing small amounts of current over long periods of time and lessening the impact of Mg^{+2} blockade. The net result of this modulation would be increased suppression of NBP activity and consequent strengthening of inhibitory surrounds. Such a form of modulation would also serve to explain the absence of Apt. NMDAR2D message in the GCL of the LS where the need for large receptive fields with weak inhibitory surrounds would necessitate a lower basal rate of granule cell activity.

Summary

Partial cDNAs for each of the four known NMDAR2 subunits have been cloned from the brain of the weakly electric fish *Apteronotus leptorhynchus*. These clones were obtained through a combination of conventional cDNA library screens and RT-PCR. Preliminary sequence analysis has revealed that each of the apteronotid NMDAR2 cDNAs displays a high degree of sequence homology with its mammalian counterpart. Observed homologies are highest in the region spanning the transmembrane/re-entrant loop domains M1-M4 (78-81% amino acid identity). Analysis of Apt. NMDAR2C and Apt. NMDAR2D cDNAs indicate that these sequences may diverge sharply from those of their mammalian homologues in regions 3' of the fourth transmembrane domain (M4).

Analysis of Apt. NMDAR2 transcript expression in the ELL has revealed a complex, yet discrete pattern of distribution for each of the subunit mRNAs. Apt. NMDAR2A message has been found present throughout the depth of the pyramidal and granule cell layers of all segments. Apt. NMDAR2B mRNA has been detected throughout the granule cell layer of all segments but is apparently restricted to a superficial sub-population of pyramidal cells. Apt. NMDA2C transcript is present in low levels throughout the granule cell layers of all segments. However, its expression in the pyramidal cell layer is segmentally regulated, being high in cells of the MS, CMS, and CLS but significantly lower in those of the LS. Apt. NMDAR2D transcript has been detected at high levels in sites of cell proliferation (EGm) and in granule cells of the ELL where it is present in a mediolateral gradient.

References

Aizenman, E., Lipton, S. A., and Loring, R. H. (1989). Selective modulation of NMDA responses by reduction and oxidation. *Neuron* 2, 1257-1263.

Appel, S. H. (1993). Excitotoxic neuronal cell death in amyotrophic lateral sclerosis. *TINS* 16, 3-5.

Ascher, P. (1998). Zinc, *Src* and NMDA receptors-a transmembrane connection. *Nature Neurosci.* 1, 173-175.

Audinet, E., Lambolez, B., Rossier, J., and Crepel, F. (1994). Activity-dependent regulation of N-methyl-D-aspartate receptor subunit expression in rat cerebellar granule cells. *Euro. J. Neurosci.* 6, 1792-1800.

Bastian, J. (1981). Electrolocation. I. How the electroreceptors of *Apteronotus albifrons* code for moving objects and other electrical stimuli. *J. Comp. Physiol.* 144, 465-479.

Bastian, J. (1986). Gain control in the electrosensory system: a role for the descending projections to the electrosensory lateral line lobe. *J. Comp. Physiol. [A]* 158, 505-515.

Bastian, J. (1993). The role of amino acid neurotransmitters in the descending control of electroreception. *J. Comp. Physiol. [A]* 172, 409-423.

Bastian, J., and Courtright, J. (1991). Morphological correlates of pyramidal cell adaptation rate in the electrosensory lateral line lobe of weakly electric fish. *J. Comp. Physiol. [A]* 168, 393-407.

Behar, T. N., Scott, C. A., Greene, C. L., Wen, X., Smith, S. V., Maric, D., Liu, Q. Y., Colton, C. A., and Barker, J. L. (1999). Glutamate acting at NMDA receptors stimulates embryonic cortical neuronal migration. *J. Neurosci.* 19, 4449-4461.

Benveniste, M., Clements, J., Vyklicky, L., and Mayer, M. L. (1990). A kinetic analysis of the modulation of N-methyl-D-aspartic acid receptors by glycine in mouse cultured hippocampal neurones. *J. Physiol. Lond.* 428, 333-357.

Benveniste, M., and Mayer, M. L. (1991). Kinetic analysis of antagonist action at N-methyl-D-aspartic acid receptors. Two binding sites each for glutamate and glycine. *Biophys. J.* 59, 560-573.

Benveniste, M., and Mayer, M. L. (1993). Multiple effects of spermine on N-methyl-D-aspartic acid receptor responses of rat cultured hippocampal neurones. *J. Physiol. Lond.* 464, 131-163.

Berman, N. J., Hincke, M. T., and Maler, L. (1995). Inositol 1,4,5-triphosphate receptor localization in the brain of a weakly electric fish (*Apteronotus leptorhynchus*) with emphasis on the electrosensory system. *J. Comp. Neurol.* 361, 512-524.

Berman, N. J., Plant, J., Turner, R. W., and Maler, L. (1997). Excitatory amino acid receptors at a feedback pathway in the electrosensory system: implications for the searchlight hypothesis. *J. Neurophysiol.* **78**, 1869-1881.

Bliss, T. V. P., and Collingridge, G. L. (1993). A synaptic model of memory: long-term potentiation in the hippocampus. *Nature* **361**, 31-39.

Bottai, D., Dunn, R. J., Ellis, W., and Maler, L. (1997). N-methyl-D-aspartate receptor 1 mRNA distribution in the central nervous system of the weakly electric fish *Apteronotus leptorhynchus*. *J. Comp. Neurol.* **389**, 65-80.

Bottai, D., Maler, L., and Dunn, R. J. (1998). Alternative RNA splicing of the NMDA receptor NR1 mRNA in the neurons of the teleost electrosensory system. *J. Neurosci.* **18**, 5191-5202.

Buller, A. L., Larson, H. C., Schneider, B. E., Beaton, J. A., Morrisett, R. A., and Monaghan, D. T. (1994). The molecular basis of NMDA receptor subtypes: native receptor diversity is predicted by subunit composition. *J. Neurosci.* **14**, 5471-5484.

Bullock, T. H. (1969). Species differences in effect of electroreceptor input on electric organ pacemakers and other aspects of behavior in electric fish. *Brain, Behav. and Evol.* **2**, 85-118.

Bunrashev, N., Monyer, H., Seeburg, P. H., and Sakmann, B. (1992). Divalent ion permeability of AMPA receptor channels is dominated by the edited form of a single subunit. *Neuron* 8, 189-198.

Carimignoto, G., and Vicini, S. (1992). Activity-dependent decrease in NMDA receptor responses during development of the visual cortex. *Science* 258, 1007-1011.

Carr, C. E., Heiligenberg, W., and Rose, G. J. (1986). A time-comparison circuit in the electric fish midbrain. I. Behaviour and Physiology. *J. Neurosci.* 6, 107-119.

Chen, L., and Huang, L. Y. M. (1992). Protein kinase C reduces Mg^{+2} block of NMDA-receptor channels as a mechanism of modulation. *Nature* 356, 521-523.

Chen, L., and Huang, L. Y. M. (1991). Sustained potentiation of NMDA receptor-mediated glutamate responses through activation of protein kinase C by a μ -opioid. *Neuron* 7, 319-326.

Chen, N., Luo, T., and Raymond, L. A. (1999). Subtype dependence of NMDA receptor channel open probability. *J. Neurosci.* 19, 6844-6954.

Chen, N., Moshaver, A., and A., R. L. (1997). Differential sensitivity of recombinant N-methyl-D-aspartate receptor subtypes to zinc inhibition. *Mol. Pharmacol.* 51, 1015-1023.

Christine, C. W., and Choi, D. W. (1990). Effect of zinc on NMDA receptor-mediated channel currents in cortical neurons. *J. Neurosci.* *10*, 108-116.

Crick, F. (1984). Function of the thalamic reticular complex: the searchlight hypothesis. *Proc. Natl. Acad. Sci. USA* *81*, 4586-4590.

Daw, N. W., Stein, P. S. G., and Fox, K. (1993). The role of NMDA receptors in information processing. *Annu. Rev. Neurosci.* *16*, 207-222.

Durand, G. M., Bennett, M. V. L., and Zukin, R. S. (1993). Splice variants of the N-methyl-D-aspartate receptor NR1 identify domains involved in regulation by polyamines and protein kinase C. *Proc. Natl. Acad. Sci. USA* *90*, 6731-6735.

Durand, G. M., Gregor, P., Zheng, X., Bennett, M. V. L., Uhl, G. R., and Zukin, R. S. (1992). Cloning of an apparent splice variant of the rat N-methyl-D-aspartate receptor NMDAR1 with altered sensitivity to polyamines and activators of protein kinase C. *Proc. Natl. Acad. Sci. USA* *89*, 9359-9363.

Dye, J. C., Heiligenberg, W., Keller, C. H., and Kawasaki, M. (1989). Different classes of glutamate receptors mediate distinct behaviors in a single brainstem nucleus. *Proc. Natl. Acad. Sci. USA* *86*, 8993-8997.

Dzubay, J. A., and Jahr, C. E. (1996). Kinetics of NMDA channel opening. *J. Neurosci.* *16*, 4129-4134.

Edmonds, B., Gibb, A. J., and Colquhoun, D. (1995). Mechanisms of activation of glutamate receptors and the time course of excitatory synaptic events. *Annu. Rev. Physiol.* *57*, 495-519.

Ehlers, M. D., Mammen, A. L., Lau, L. F., and Huganir, R. L. (1996a). Synaptic targeting of glutamate receptors. *Curr. Opin. Cell Biol.* *8*, 484-489.

Ehlers, M. D., Zhang, S., Bernhardt, J. P., and Huganir, R. L. (1996b). Inactivation of NMDA receptors by direct interaction of calmodulin with the NR1 subunit. *Cell* *84*, 745-755.

Farrant, M., and Cull-Candy, S. G. (1991). Excitatory amino acid receptor channels in Purkinje cells in thin cerebellar slices. *Proc. R. Soc. London [Biol.]* *244*, 179-184.

Farrant, M., Feldmeyer, D., Takahashi, T., and Cull-Candy, S. G. (1994). NMDA-receptor channel diversity in the developing cerebellum. *Nature* *368*, 335-339.

Finger, T. E., Bell, C. C., and Carr, C. E. (1986). Why are Electrosensory Systems So Similar? In *Electroreception.*, T. H. Bullock, and Heiligenberg, W., ed. (New York: Wiley), pp. 465-481.

Flint, A. C., Maisch, U. S., Weishaupt, J. H., Kreigstien, A. R., and Monyer, H. (1997). NR2A subunit expression shortens NMDA receptor synaptic currents in developing neocortex. *J. Neurosci.* *17*, 2469-2476.

Fox, K. (1995). The critical period for long-term potentiation in primary sensory cortex. *Neuron* *15*, 485-488.

Fox, K., Henley, J., and Isaac, J. (1999). Experience-dependent development of NMDA receptor transmission. *Nature Neurosci.* *2*, 297-299.

Garthwaite, G., Yamini, B., and Garthwaite, J. (1987). Selective loss of Purkinje and granule cell responsiveness to N-methyl-D-aspartate in rat cerebellum during development. *Brain Res.* *433*, 288-292.

Gerber, G., Kangara, I., Ryu, P. D., Larew, J. S., and Randic, M. (1989). Multiple effects of phorbol esters in the rat dorsal spinal horn. *J. Neurosci.* *9*, 3606-3617.

Heiligenberg, W. (1990). Electrosensory systems in fish. *Synapse* *6*, 196-206.

Heiligenberg, W., and Dye, J. (1982). Labelling of electroreceptive afferents in a gymnotid fish by intracellular injection of HRP: the mystery of multiple maps. *J. Comp. Physiol. [A]* *148*, 287-296.

Hollmann, M., and Heinemann, S. (1994). Cloned glutamate receptors. *Annu. Rev. Neurosci.* *17*, 31-108.

Ishii, T., Moriyoshi, K., Sugihara, K., Kadotani, H., Yokoi, M., Akazawa, C., Shigemoto, R., Mizuno, N., Masu, M., and S., N. (1993). Molecular characterization of the family of the N-methyl-D-aspartate receptor subunits. *J. Biol. Chem.* *268*, 2836-2843.

Kawasaki, M. (1996). Comparative analysis of the jamming avoidance response in african and south american wave-type electric fishes. *Biol. Bull.* *191*, 103-108.

Kawasaki, M. (1997). Sensory hyperacuity in the jamming avoidance response of weakly electric fish. *Curr. Opin. Neurobiol.* *7*, 473-479.

Kennedy, M. B. (1993). The postsynaptic density. *Curr. Opin. Neurobiol.* *3*, 732-737.

Kim, E., Cho, K. O., Rothschild, A., and Sheng, M. (1996). Heteromultimerization and NMDA receptor-clustering activity of Chapsyn-110, a member of the PSD-95 family of proteins. *Neuron* *17*, 103-113.

Kim, E., Niethammer, M., Rothschild, A., Jan, Y. N., and Sheng, M. (1995). Clustering of Shaker-type K⁺ channels by interaction with a family of membrane-associated guanylate kinases. *Nature* *378*, 85-88.

Kirkwood, A., Rioult, M. G., and Bear, M. F. (1996). Experience-dependent modification of synaptic plasticity in visual cortex. *Nature* *381*, 526-528.

Kornau, H., Schenker, L. T., Kennedy, M. B., and Seeburg, P. H. (1995). Domain interaction between NMDA receptor subunits and the post-synaptic density protein PSD-95. *Science* *269*, 1737-1740.

Kuner, T., and Schoepfer, R. (1996). Multiple structural elements determine subunit specificity of Mg^{+2} block in NMDA receptor channels. *J. Neurosci.* *16*, 3549-3558.

Kutsuwada, T., Kashiwabuchi, N., Mori, H., Sakimura, K., Kushiya, E., Araki, K., Meguro, H., Masaki, H., Kumanishi, T., Arakawa, M., and Mishina, M. (1992). Molecular diversity of the NMDA receptor channel. *Nature* *358*, 36-41.

Laube, B., Kuhse, J., and Betz, H. (1998). Evidence for a tetrameric structure of recombinant NMDA receptors. *J. Neurosci.* *18*, 2954-2961.

Legendre, P., Rosemund, C., and Westbrook, G. L. (1993). Inactivation of NMDA channels in cultured hippocampal neurons by intracellular calcium. *J. Neurosci.* *13*, 674-684.

Legendre, P., and Westbrook, G. L. (1991). Ifenprodil blocks N-methyl-D-aspartate receptors by a two-component mechanism. *Mol. Pharmacol.* *40*, 289-298.

Legendre, P., and Westbrook, G. L. (1990). The inhibition of single N-methyl-D-aspartate-activated channels by zinc on cultured rat neurones. *J. Physiol. Lond.* **429**, 429-449.

Leonard, A. S., Lim, I. A., Hemsworth, D. E., Horne, M. C., and Hell, J. W. (1999). Calcium/calmodulin-dependent protein kinase II is associated with the N-methyl-D-aspartate receptor. *Proc. Natl. Acad. Sci. USA* **96**, 3239-3244.

Li, W.-H., and Graur, D. (1991). *Fundamentals of molecular evolution.* (Sunderland, Massachusetts: Sinauer Associates, Inc.).

Lin, J. W., Wyszynski, M., Madhavan, R., Sealock, R., Kim, J. U., and Sheng, M. (1998). Yotiao, a novel protein of neuromuscular junction and brain that interacts with specific splice variants of NMDA receptor subunit NR1. *J. Neurosci.* **18**, 2017-2027.

Lu, Y. M., Roder, J. C., Davidow, J., and Salter, M. W. (1998). *Src* activation in the induction of long-term potentiation in CA1 hippocampal neurons. *Science* **279**, 1363-1367.

MacDonald, J. F., Mody, I., and Salter, M. W. (1989). Regulation of N-methyl-D-aspartate receptors revealed by intracellular dialysis of murine neurones in culture. *J. Physiol. Lond.* **414**, 17-34.

Maler, L., and Monaghan, D. (1991). The distribution of excitatory amino acid binding sites in the brain of an electric fish, *Apteronotus leptorhynchus*. *J. Chem. Neuroanat.* **4**, 36-61.

Maler, L., Sas, E., Johnston, S., and Ellis, W. (1991). An atlas of the brain of the electric fish *Apteronotus leptorhynchus*. *J. Chem. Neuroanat.* **4**, 1-38.

McBain, C. J., and Mayer, M. L. (1994). N-methyl-D-aspartic acid receptor structure and function. *Physiol. Rev.* **74**, 723-760.

McGurk, J. F., Bennett, M. V., and Zukin, R. S. (1990). Polyamines potentiate responses of N-methyl-D-aspartate receptors expressed in *Xenopus* oocytes. *Proc. Natl. Acad. Sci. USA* **87**, 9971-9974.

Meldrum, B., and Garthwaite, J. (1990). Excitatory amino acid neurotoxicity and neurodegenerative disease. *Trends Pharmacol. Sci.* **11**, 379-387.

Metzner, W., and Juranek, J. (1997). A sensory brain map for each behavior? *Proc. Natl. Acad. Sci. USA* **94**, 14798-14803.

Metzner, W., Koch, C., Wessel, R., and Gabbiani, F. (1998). Feature extraction by burst-like spike patterns in multiple sensory maps. *J. Neurosci.* **18**, 2283-2300.

Miyakawa, T., Yagi, T., Kitazawa, H., Yasuda, M., Kawai, N., Tsuboi, K., and Niki, H. (1997). *Fyn*-kinase as a determinant of ethanol

sensitivity: relation to NMDA-receptor function. *Science* 278, 698-701.

Montgomery, J. C., Coombs, S., Conley, R. A., and Bodznick, D. (1995). Hindbrain sensory processing in lateral line, electrosensory, and auditory systems: a comparative overview of anatomical and functional similarities. *Aud. Neurosci* 1, 207-231.

Monyer, H., Burnashev, N., Laurie, D. J., Sakmann, B., and Seeburg, P. H. (1994). Developmental and regional expression in the rat brain and functional properties of four NMDA receptors. *Neuron* 12, 529-540.

Moon, S. I., Apperson, M. L., and Kennedy, M. B. (1994). The major tyrosine-phosphorylated protein in the postsynaptic density fraction is the N-methyl-D-aspartate receptor subunit 2B. *Proc. Natl. Acad. Sci. USA* 91, 3954-3958.

Mountcastle, V. (1967). The problem of sensing and the neural coding of sensory events. In *The Neurosciences: A Study Program.*, G. C. Qualton, Melnechuk, T., and Schmitt, F. O., ed. (New York: The Rockefeller University Press), pp. 393-408.

Nakanishi, N., Axel, R., and Shneider, N. A. (1992a). Alternative splicing generates functionally distinct N-methyl-D-aspartate receptors. *Proc. Natl. Acad. Sci. USA* 89, 8552-8556.

Nakanishi, S. (1992b). Molecular diversity of glutamate receptors and implications for brain function. *Science* 258, 597-603.

Nelson, S. B., and Sur, M. (1992). NMDA receptors in sensory information processing. *Curr. Opin. Neurobiol.* **2**, 484-488.

Niedzielski, A. S., and Wenthold, R. J. (1995). Expression of AMPA, Kainate, and NMDA receptor subunits in cochlear and vestibular ganglia. *J. Neurosci.* **15**, 2338-2353.

Niethammer, M., Kim, E., and Sheng, M. (1996). Interaction between the C terminus of NMDA receptor subunits and multiple members of the PSD-95 family of membrane-associated guanylate kinases. *J. Neurosci.* **16**, 2157-2163.

O'Dell, T. J., Kandel, E. R., and Grant, S. G. N. (1991). Long-term potentiation in the hippocampus is blocked by tyrosine kinase inhibitors. *Nature* **353**, 558-560.

Petralia, R. S., Wang, Y. X., and Wenthold, R. J. (1994). The NMDA receptor subunits NR2A and NR2B show histological and ultrastructural localization patterns similar to those of NR1. *J. Neurosci.* **14**, 6102-6120.

Pettigrew, J. D. (1999). Electroreception in monotremes. *J. Exp. Biol.* **202**, 1447-1454.

Pettigrew, J. D., Manger, P. R., and Fine, S. L. (1998). The sensory world of the platypus. *Phil. Trans. Royal Soc. London [B]* **353**, 1199-1210.

Quinlan, E. M., Philpot, B. D., Huganir, R. L., and Bear, M. F. (1999). Rapid, experience-dependent expression of synaptic NMDA receptors in visual cortex *in vivo*. *Nature Neurosci.* *2*, 352-357.

Raymond, L. A., Blackstone, C. D., and Huganir, R. L. (1993). Phosphorylation of amino acid neurotransmitter receptors in synaptic plasticity. *TINS* *16*, 147-153.

Roberts, E. B., Meredith, M. A., and Ramoa, A. S. (1998). Suppression of NMDA receptor function using antisense DNA blocks ocular dominance plasticity while preserving visual responses. *J. Neurophysiol.* *80*, 1021-1032.

Roche, K. W., Ly, C. D., Petralia, R. S., Wang, Y.-X., McGee, A. W., Bredt, D. S., and Wenthold, R. J. (1999). Postsynaptic density-93 interacts with the $\delta 2$ glutamate receptor subunit at parallel fibre synapses. *J. Neurosci.* *19*, 3926-3934.

Rock, D. M., and Mac Donald, R. L. (1992a). The polyamine spermine has multiple actions on N-methyl-D-aspartate receptor single-channel currents in cultured cortical neurons. *Mol. Pharmacol.* *41*, 83-88.

Rock, D. M., and MacDonald, R. L. (1992b). Spermine and related polyamines produce a voltage-dependent reduction of N-methyl-D-aspartate receptor single-channel conductance. *Mol. Pharmacol.* *42*, 157-164.

Rosenmund, C., Legendre, P., and Westbrook, G. L. (1992). Expression of NMDA channels on cerebellar Purkinje cells acutely dissociated from newborn rats. *J. Neurosci.* **68**, 1901-1905.

Sala, C., and Sheng, M. (1999). The *fyn* art of N-methyl-D-aspartate receptor phosphorylation. *Proc. Natl. Acad. Sci. USA* **96**, 335-337.

Sambrook, J., Fritsch, E. F., and Maniatis, T. (1989). *Molecular Cloning: a laboratory manual.*, 2nd ed. Edition, Volume 1 (Cold Spring Harbour, NY: Cold Spring Harbour Laboratory Press).

Saunders, J., and Bastian, J. (1984). The physiology and morphology of two types of electrosensory neurons in the weakly electric fish *Apteronotus leptorhynchus*. *J. Comp. Physiol. [A]* **154**, 199-209.

Seeburg, P. H., Burnashev, N., Kohr, G., Kuner, T., Sprengel, R., and Monyer, H. (1995). The NMDA receptor channel: molecular design of a coincidence detector. *Rec. Prog. Hor. Res.* **50**, 19-34.

Sheng, M., Cummings, J., Roldan, L. A., Jan, Y. N., and Jan, Y. J. (1994). Changing subunit composition of heteromeric NMDA receptors during the development of rat cortex. *Nature* **368**, 144-147.

Shumway, C. A. (1989b). Multiple electrosensory maps in the medulla of weakly electric gymnotiform fish. II. anatomical differences. *J. Neurosci.* **9**, 4400-4415.

Shumway, C. A. (1989a). Multiple electrosensory maps in the medulla of weakly electric gymnotiform fish. I. physiological differences. *J. Neurosci.* **9**, 4388-4399.

Smith, K. E., Borden, L. A., Hartig, P. R., Branchek, T., and Weinshank, R. L. (1992). Cloning and expression of a glycine transporter reveal colocalization with NMDA receptors. *Neuron* **8**, 927-935.

Smart, T. G. , Xie, X., and Krishek, B. J. (1994). Modulation of inhibitory and excitatory amino acid receptor ion channels by zinc. *Prog. Neurobiol.* **42**, 393-441.

Sprengel, R., Suchanek, B., Amico, C., Brusa, R., Burnashev, N., Rosov, A., Hvalby, O., Jensen, V., Paulsen, O., Andersen, P., Kim, J. J., Thompson, R. F., Sun, W., Webster, L. C., Grant, S. G. N., Eilers, J., Konnerth, A., Li, J., McNamara, J. O., and Seeburg, P. H. (1998). Importance of the intracellular domain of NR2 subunits for NMDA receptor function *in vivo*. *Cell* **92**, 279-289.

Takahashi, T., Feldmeyer, D., Suzuki, N., Onodera, K., Cull-Candy, S. G., Sakimura, K., and Mishina, M. (1996). Functional correlation of NMDA receptor ϵ subunits expression with the properties of single-channel and synaptic currents in the developing cerebellum. *J. Neurosci.* **16**, 4376-4382.

Tang, C. M., Dichter, M., and Morad, M. (1990). Modulation of the N-methyl-D-aspartate channel by extracellular H^+ . *Proc. Natl. Acad. Sci. USA* **87**, 6445-6449.

Tezuka, T., Umemori, H., Akiyama, T., Nakanishi, S., and Yamamoto, T. (1999). PSD-95 promotes *Fyn*-mediated tyrosine phosphorylation of the N-methyl-D-aspartate receptor subunit NR2A. *Proc. Natl. Acad. Sci. USA* 96, 435-440.

Traynelis, S. F., and Cull-Candy, S. G. (1990). Proton inhibition of N-methyl-D-aspartate receptors in cerebellar neurons. *Nature Lond.* 345, 347-350.

Vicini, S., Wang, J. F., Li, J. H., Zhu, W. J., Wang, Y. H., Luo, J. H., Wolfe, B. B., and Grayson, D. R. (1998). Functional and pharmacological differences between recombinant N-methyl-D-aspartate receptors. *J. Neurophysiol.* 79, 555-566.

Wanatabe, M., Inoue, Y., Sakimura, K., and Mishina, M. (1992). Developmental changes in distribution of NMDA receptor channel subunit mRNAs. *Neuroreport* 3, 1138-1140.

Wanatabe, M., Mishina, M., and Inoue, I. (1994). Distinct spatiotemporal pattern of five NMDA receptor channel subunit mRNAs in the cerebellum. *J. Comp. Neurol.* 343, 513-519.

Wang, Y. T., and Salter, M. W. (1994). Regulation of NMDA receptors by tyrosine kinases and phosphatases. *Nature* 369, 233-235.

Westbrook, G. L., and Mayer, M. L. (1987). Micromolar concentrations of Zn^{+2} antagonize NMDA and GABA responses of hippocampal neurons. *Nature Lond.* **328**, 640-643.

Williams, K., Russell, S. L., Shen, Y. M., and Molinoff, P. B. (1993). Developmental switch in the expression of NMDA receptors occurs *in vivo* and *in vitro*. *Neuron* **10**, 267-278.

Wong, C. J. H. (1997). Afferent and efferent connections of the diencephalic prepacemaker nucleus in the weakly electric fish, *Eigemannia virescens*: interactions between the electromotor system and the neuroendocrine axis. *J. Comp. Neurol.* **383**, 18-41.

Wyszynski, M., Lin, J., Rao, A., Nigh, E., Beggs, A. H., Craig, A. M., and Sheng, M. (1997). Competitive binding of α -actinin and calmodulin to the NMDA receptor. *Nature* **385**, 439-442.

Yu, X. M., Askalan, R., Keil II, G. J., and W., S. M. (1997). NMDA channel regulation by channel-associated protein tyrosine kinase *Src*. *Science* **275**, 674-678.

Yuste, R., Majewska, A., Cash, S. S., and Denk, W. (1999). Mechanisms of calcium influx into hippocampal spines: heterogeneity among spines, coincidence detection by NMDA receptors, and optical quantal analysis. *J. Neurosci.* **19**, 1976-1986.

Zhang, S., Ehlers, M. D., Bernhardt, J. P., Su, C. T., and Huganir, R. L. (1998). Calmodulin mediates calcium-dependent inactivation of N-methyl-D-aspartate receptors. *Neuron* 21, 443-453.

Zheng, F., Gingrich, M. B., Traynelis, S. F., and Conn, P. J. (1998). Tyrosine kinase potentiates NMDA receptor currents by reducing tonic zinc inhibition. *Nature Neurosci.* 1, 185-191.

Zukin, R. S., and Bennett, M. V. (1995). Alternatively spliced isoforms of the NMDAR1 receptor subunit. *TINS* 18, 306-313.

Zupanc, G. K., and Horschke, I. (1995). Proliferation zones in the brain of adult gymnotiform fish: a quantitative mapping study. *J. Comp. Neurol.* 353, 213-233.

Zupanc, G. K., and Zupanc, M. M. (1992b). Birth and migration of neurons in the central posterior/prepacemaker nucleus during adulthood in weakly electric knifefish. *Proc. Natl. Acad. Sci. USA* 89, 9539-9543.

Zupanc, G. K. H. (1999). Neurogenesis, cell death and regeneration in the adult gymnotiform fish. *J. Exp. Biol.* 202, 1435-1446.

Zupanc, G. K. H., Airey, L., Maler, L., Sutko, J., and Ellisman, M. H. (1992a). Immunohistochemical localization of ryanodine binding proteins in the central nervous system of gymnotiform fish. *J. Comp. Neurol.* 325, 135-151.